TECHNICAL REPORT No. 42

ON LONG STATIONARY AND TRANSIENT ATMOSPHERIC WAVES

by

A.C. Wiin - Nielsen*

* Visiting Scientist
Present affiliation:
Danish Meteorological Institute
Copenhagen, Denmark.

August 1984

C O N T E N T S

Abstract

The structure of long stationary and transient waves in the atmosphere is studied using a quasi-geostrophic, two level model and spherical geometry. The waves are forced by heating or orography.

The solutions for stationary waves influenced by heating show that the amplitudes and slopes are determined mainly by the strength of the zonal wind. Weak zonal winds create an eastward slope with height and strong zonal winds a westward slope. The transition from one slope to the opposite slope occurs for a value of 5-6 of the meridional index for weak zonal winds and for 2-3 for strong zonal winds. The amplitudes are largest in the neighbourhood of the transition. These maxima in the amplitude may be explained as resonance phenomena. The energetics of the long stationary waves is analysed in detail showing that the total production of available potential energy of the waves is always positive, but that the conversion from zonal available potential energy is negative for the eastward sloping waves.

The theoretical study is compared with the structure of the waves as obtained from climatological maps for the Northern Hemisphere for January and July using spherical harmonic analysis with favourable results.

The forcing of long stationary waves by orography is considered using the same technique as earlier and with analogous results.

Finally, the transient waves are analysed using a stability analysis showing that the unstable case leads to a westward slope with height while the stable case has the opposite slope.

1. INTRODUCTION

This study is concerned with the structure of long waves in the troposphere. A Fourier analysis of the height field of the normal maps for the Northern Hemisphere along a middle latitude circle (50°N) shows that the waves with wave number 1, 2 and 3 slope to the west in the winter and to the east in the summer, (Eliassen, 1958). An investigation of the structure of the long stationary waves was made by Wiin-Nielsen (1961) using the vorticity equation for the vertical mean flow in the stationary case. From this equation it is possible to investigate the distribution of temperature relative to height in the stationary planetary waves. On the other hand the investigation did not give any results concerning the absolute position of the long, stationary waves because the vorticity equation for the vertical shear flow was disregarded. The reason for the neglect of the equation for the shear flow was that this equation contains the heating of the atmosphere, and it was not possible at the time to give a realistic specification of the heating.

Investigation by Saltzman (1968) and Wiin-Nielsen (1972) have shown that the heating in a two-level model including short-wave solar radiation, long-wave outgoing radiation, small-scale convection, evaporation and condensation, latent heat release and subsurface conduction may be formulated in a parameterized form, and it was demonstrated by Wiin-Nielsen (loc.cit.) that the heating function may be formulated in a Newtonian form where the coefficient of intensity and the equilibrium temperature field can be calculated from the parameterization formulas. This formulation will be used in the model to be described later.

With this formulation of the heating and with the incorporation of dissipation in the planetary boundary layer and in the free atmosphere it is possible to solve the stationary linearized equations for a two-level quasi-geostrophic model. The model will be formulated on the spherical earth and linearization will be around a zonal flow with constant angular velocity. It will furthermore be convenient to find the solutions in terms of spherical harmonics. The investigation is in this regard similar to a large number of other studies which attempt to calculate the atmospheric response to heating. Smagorinsky (1953) initiated such studies. The response as a function of scale is important particularly because of the recent interest in the influence of anomalous heating on the atmospheric circulation, as for example the effects of the heat source created by the El Niño phenomenon.

The study of the long stationary waves is described in Sects. 2 to 5 of which Sect.2 contains the formulation of the problem, Sect.3 gives a description of the solutions and discusses the results, Sect.4 discusses the vertical structure and the energetics of the waves, and Sect.5 contains a comparison between the theoretical results and results from a decomposition of climatological maps for January and July in spherical harmonics showing good agreement between theory and observations.

Sect.6 contains a discussion of the long stationary waves as forced by topography which was disregarded in the previous sections. The main result is that the mountain forcing acts qualitatively in the same way as forcing by heat sources in the sense that the slope in the vertical direction of the waves is controlled by the zonal wind speeds. For small values of the zonal wind speeds the waves slope eastward with height for sufficiently small values of the meridional index. Stronger zonal winds limit the eastward sloping waves to smaller values of the meridional index.

In Sect.7 we leave the problem of stationary waves and give a brief analysis of the stability of transient long waves on the spherical earth including heating and dissipation. This study supplements the investigation of the stationary waves and extends earlier studies to a spherical geometry.

Sect.8 contains a summary and concluding remarks.

2. THE LINEARIZED MODEL

As indicated in the introduction we shall specify the heating in a Newtonian form:

$$H = - \gamma C_p (T - T_E) \tag{2.1}$$

in which H is the heating per unit mass and unit time, γ is the coefficient of intensity, C_p the specific heat at constant pressure, T the temperature and T_E the so-called equilibrium temperature.

The dissipation is formulated in agreement with the model used by Wiin-Nielsen (1972), and the basic equations may be obtained from that study by setting the time-derivations to zero.

As mentioned in the introduction we shall linearize around a zonal flow with constant angular velocity. The linear velocities of the mean flow and the shear flow are, respectively,

$$U_* = a \cos\phi \, \Lambda_* \; ; \; U_T = a \cos\phi \, \Lambda_T \tag{2.2}$$

and the corresponding relative velocities are:

$$\bar{\zeta}_* = 2\Lambda_* \mu ; \quad \bar{\zeta}_T = 2\Lambda_T \mu \; , \; \mu = \sin\phi \tag{2.3}$$

With these notations we may write the steady state equations for mean flow and the shear flow as follows:

$$\Lambda_* \frac{\partial \nabla^2\psi'_*}{\partial\lambda} + \Lambda_T \frac{\partial \nabla^2\psi'_T}{\partial\lambda} + \frac{2(\Omega+\Lambda_*)}{a^2}\frac{\partial\psi'_*}{\partial\lambda} + \frac{2\Lambda_T}{a^2}\frac{\partial\psi'_T}{\partial\lambda} = -\frac{1}{2}\varepsilon(\nabla^2\psi'_*-2\nabla^2\psi'_T)$$

$$\Lambda_* \frac{\partial \nabla^2\psi'_T}{\partial\lambda} + \Lambda_T \frac{\partial \nabla^2\psi'_*}{\partial\lambda} + \frac{2\Lambda_T}{a^2}\frac{\partial\psi'_*}{\partial\lambda} + \frac{2(\Omega+\Lambda_*)}{a^2}\frac{\partial\psi'_T}{\partial\lambda} = \frac{f_o}{P}\ \omega - 2\nu\ \nabla^2\psi'_T + \frac{1}{2}\varepsilon(\nabla^2\psi'_*-2\nabla^2\psi'_T) \qquad (2.4)$$

while the thermodynamic equation may be written in the form:

$$\frac{f_o}{P}\omega = \lambda^2\left[\Lambda_* \frac{\partial\psi'_T}{\partial\lambda} - \Lambda_T \frac{\partial\psi'_*}{\partial\lambda}\right] + \lambda^2\ \gamma\ (\psi'_T - \psi'_E) \qquad (2.5)$$

When (2.5) is substituted in the last equation in the system (2.4) we obtain two equations in the dependent variables ψ'_* and ψ'_T. In solving these linear equations it is convenient to non-dimensionalize the dependent variables. The perturbation streamfunctions are written in the form:

$$\begin{bmatrix} \psi'_* \\ \psi'_T \\ \psi'_E \end{bmatrix} = a^2\Omega \begin{bmatrix} \eta_* \\ \eta_T \\ \eta_E \end{bmatrix} \qquad (2.6)$$

With this scaling we may write the vorticity in the form:

$$\nabla^2\psi' = \Omega\left\{\frac{1}{1-\mu^2}\frac{\partial^2\eta}{\partial\lambda^2} + \frac{\partial}{\partial\mu}\left[(1-\mu^2)\frac{\partial\eta}{\partial\mu}\right]\right\} \qquad (2.7)$$

It is furthermore decided to seek solutions in terms of the spherical harmonic functions, i.e.

$$\begin{bmatrix} \eta_* \\ \eta_T \\ \eta_E \end{bmatrix} = \begin{bmatrix} A_* \\ A_T \\ A_E \end{bmatrix} P_n^m(\mu)\ e^{im\lambda} \qquad (2.8)$$

in which m is the zonal wave number and n the meridional index. Using (2.8) we may write (2.7) as follows

$$\nabla^2\psi' = -\Omega\ n(n+1)\ A\ P_n^m(\mu)\ e^{im\lambda} = -\Omega\ C\eta \qquad (2.9)$$

in which $C = n(n+1)$.

The dependent variables are now the amplitudes $A_* = A_*(m,n)$ and $A_T = A_T(m,n)$ while the forcing is represented by A_E. The non-dimensional variables are introduced in the basic equations together with the representation (2.8). After considerable reduction we find the following equations for A_* and A_T:

$$(1 + iG)A_* - (2 - iH)\, A_T = 0 \tag{2.10}$$

$$-(1 - iK)A_* + (M + iL)\, A_T = \frac{\Gamma}{eC}\, A_E$$

in which

$$G = m\,\frac{\frac{\Lambda_*}{\Omega}\,(\tfrac{1}{2}C-1) - 1}{eC}$$

$$H = m\,\frac{\frac{\Lambda_T}{\Omega}\,(\tfrac{1}{2}C-1)}{eC}$$

$$K = m\,\frac{\frac{\Lambda_T}{\Omega}\,(\tfrac{1}{2}C-1-\tfrac{1}{2}\,\lambda^2a^2)}{eC} \tag{2.11}$$

$$L = m\,\frac{\frac{\Lambda_*}{\Omega}\,(\tfrac{1}{2}C-1+\tfrac{1}{2}\,\lambda^2a^2)-1}{eC}$$

$$M = 2 + \frac{a_T}{e} + \frac{\Gamma}{ec}$$

and $$e = \frac{\varepsilon}{4\Omega}\,,\quad a_T = \frac{\nu}{\Omega}\,,\quad \Gamma = \frac{\gamma\,\lambda^2a^2}{2\Omega} \tag{2.12}$$

Since (2.10) is a system of linear inhomogeneous equations it is straightforward to obtain the solutions for the (complex) amplitudes A_* and A_T. The remaining part of the paper will be devoted to a study of the solutions as a function of the scale parameters m and u. In this connection we shall always express the wave in the form

$$\psi = A\,\cos[m(\lambda-\theta)]\; P_n^m(\mu) \tag{2.13}$$

The phase angle θ is thus the position of the maximum of the wave having the wavelength $2\pi/m$.

The solution of (2.10) may be found in a straightforward manner. We write the final result:

$$\frac{A_T(r)}{A_E} = \frac{\Gamma}{eC}\frac{(1+G^2)Q}{Q^2+S^2} \; ; \quad \frac{A_T(i)}{A_E} = -\frac{\Gamma}{eC}\frac{(1+G^2)S}{Q^2+S^2}$$

$$\frac{A_*(r)}{A_E} = \frac{\Gamma}{eC}\frac{(2-HG)Q - (H+2G)S}{Q^2+S^2} \qquad (2.14)$$

$$\frac{A_*(i)}{A_E} = -\frac{\Gamma}{eC}\frac{(2-HG)S + (H+2G)Q}{Q^2+S^2}$$

where

$$Q = M(1+G^2) + H(G+K) + 2GK - 2 \qquad (2.15)$$

$$S = L(1+G^2) + 2(G+K) + H(1-KG)$$

3. THE SOLUTIONS

In evaluating the solutions it is necessary to assign numerical values to the various constants. The value of ε is about 3×10^{-6} s^{-1} from which it follows that

$$e \simeq 0.01$$

For A we may adopt the value $A = 6 \times 10^{-7}$ s^{-1} which leads to

$$a_T \simeq 0.008$$

The evaluation of Γ is based on the values $\gamma = 1.4 \times 10^{-6}$ s^{-1}, $\lambda^2 = 2.5 \times 10^{-12}$ m^{-2}, $a = (2/\pi) \times 10^7 m$, $\Omega = 7.29 \times 10^{-5}$ s^{-1}. With these values we obtain

$$\Gamma \simeq 1$$

Λ_* and Λ_T measure the strengths of the zonal winds. According to (2.2) we have in general

$$\Lambda = \frac{U}{a \cos \phi} \tag{3.1}$$

Measuring U at 45°N we find for $U_{45} = 10$ ms^{-1} that $\Lambda = 2.2 \times 10^{-6}$ s^{-1}. This calculation indicates the order of magnitude to be selected for Λ_* and Λ_T.

We may start by considering a number of special cases. The first case is the one when n and therefore C is very large. It is then seen from (2.11) that

$$G \simeq \frac{m}{e} \frac{\Lambda_*}{2\Omega} \; ; \; H \simeq \frac{m}{e} \frac{\Lambda_T}{2\Omega} \tag{3.2}$$

The first equation in (2.10) is in this case:

$$A_T = \frac{(e + im \frac{\Lambda_*}{2\Omega})(2e + im \frac{\Lambda_T}{2\Omega})}{4 e^2 + (\frac{\Lambda_T}{2\Omega})^2 m^2} A_* \tag{3.3}$$

(3.3) may be used to find the difference in phase angle between A_* and A_T.

Assuming that ψ_* has a zero phase angle we find that

$$\tan \theta_T = \frac{me}{2\Omega} \frac{2\Lambda_* + \Lambda_T}{2e^2 - m^2 \frac{\Lambda_* \Lambda_T}{4\Omega^2}} \tag{3.4}$$

but e^2 is small compared to the other term in the denominator such that

$$\tan \Theta_T \cong - \frac{e}{m} \frac{\frac{\Lambda_*}{\Omega} + \frac{\Lambda_T}{2\Omega}}{\frac{\Lambda_*}{2\Omega} \cdot \frac{\Lambda_T}{2\Omega}} \tag{3.5}$$

The right hand side of (3.5) is negative for relevant values of Λ_* and Λ_T for the troposphere. An investigations of (3.3) shows that the solution is such that $\frac{1}{2}\pi \leqslant \theta_T \leqslant \pi$. If m is large also we find therefore that

$$\Theta_T = \pi - \frac{e}{m} \frac{\frac{\Lambda_*}{\Omega} + \frac{\Lambda_T}{2\Omega}}{\left(\frac{\Lambda_*}{2\Omega}\right)\left(\frac{\Lambda_T}{2\Omega}\right)} \simeq \pi \tag{3.6}$$

The phase angle difference is thus $\frac{\Theta_T}{m} \simeq \frac{\pi}{m}$, but the wave length is $\frac{2\pi}{m}$. We have thus shown that for sufficiently large m <u>and</u> n the phase angle difference between the mean wave and the thermal wave is approaching one half of the wavelength.

The next special case will be m=1, n=1, i.e. C=2. In this case we have:

$$G = - \frac{1}{2e} \ , \ H=0 \tag{3.7}$$

or

$$A_T = (\tfrac{1}{2} - i \frac{1}{4e}) A_* \tag{3.8}$$

The phase angle difference is in this case determined from

$$\tan \Theta_T = - \frac{1}{2e} \simeq - 50 \tag{3.9}$$

or $\theta_T \simeq - \frac{\pi}{2}$, which means that the thermal wave is about a quarter of a wavelength ahead of the mean wave, or that the wave with (m,n) = (1,1) is tilting from west to east in the vertical direction.

To illustrate the effects of the zonal velocities we may consider still another case (m,n)= (1,2), i.e. C=6. We obtain

$$A_T = \frac{6e - i\,(1 - \frac{2\Lambda_*}{\Omega})}{12e - i\,\frac{2\Lambda_T}{\Omega}}\,A_*$$

$$= \frac{1}{2}\,\frac{\left[36e^2 + \frac{\Lambda_T}{\Omega}\,(1-2\frac{\Lambda_*}{\Omega})\right] - i\,6e\left[1 - \frac{2\Lambda_*}{\Omega} - \frac{\Lambda_T}{\Omega}\right]}{\left[36\,e^2 + (\frac{\Lambda_T}{\Omega})^2\right]}\,A_* \qquad (3.10)$$

It is seen from (3.10) that if $\Lambda_* = \Lambda_T = 0$ we still have a negative value of the phase angle which implies that the thermal wave is ahead of the mean wave or, in other words, the wave is sloping from west to east in the vertical direction. However, for sufficiently large value of Λ_* and Λ_* the imaginary part will be positive and therefore the slope will be from east to west. The exact condition is in this particular case

$$2\Lambda_* + \Lambda_T > \Omega \qquad (3.11)$$

We have thus seen in this example that within the model it is the westerly (or positive) angular velocities which makes it possible for the wave to have a structure such that the mean wave is ahead of the thermal wave. Such a structure is always possible for sufficiently large values of Λ_* and Λ_T except for the wave (m,n) = (1,1) which always has the opposite arrangement.

The next case is the general case in which we are interested only in the phase difference between the mean wave and the thermal wave. In all cases we have used e = 0.01, $a_T = 0.008$, $\Gamma = 1$ while Λ_* and Λ_T have had the following values:

$\Lambda_* = 0$; $\Lambda_T = 0$ (Table 1a)

$\Lambda_* = 4.0 \times 10^{-6}\ s^{-1}$; $\Lambda_T = 1.5 \times 10^{-6}\ s^{-1}$ (Table 1b)

$\Lambda_* = 8.0 \times 10^{-6}\ s^{-1}$; $\Lambda_T = 3.0 \times 10^{-6}\ s^{-1}$ (Table 1c)

$\Lambda_* = 1.2 \times 10^{-5}\ s^{-1}$; $\Lambda_T = 4.5 \times 10^{-6}\ s^{-1}$ (Table 1d)

$\Lambda_* = 2.4 \times 10^{-5}\ s^{-1}$; $\Lambda_T = 9.0 \times 10^{-6}\ s^{-1}$ (Table 1e).

The calculations in these cases are shown in Table 1(a) to 1(e) showing $(\Theta_* - \Theta_T)$ expressed as a fraction of the wavelength.

Table 1a Phase difference $(\theta_* - \theta_T)$ expressed as fraction of wavelength
$\Gamma = 1$, $e = 0.01$, $a_T = 0.008$, $\Lambda_* = 0$, $\Lambda_T = 0$

m \ n	1	2	3	4	5	6	7	8	9	10
1	-0.25	-0.26	-0.27	-0.28	-0.30	-0.31	-0.33	-0.35	-0.37	-0.38
2		-0.25	-0.26	-0.27	-0.27	-0.28	-0.29	-0.30	-0.32	-0.33
3			-0.26	-0.26	-0.27	-0.27	-0.28	-0.29	-0.30	-0.31
4				-0.26	-0.26	-0.27	-0.27	-0.28	-0.29	-0.29
5					-0.26	-0.26	-0.27	-0.27	-0.28	-0.28
6						-0.26	-0.26	-0.27	-0.27	-0.28
7							-0.26	-0.27	-0.27	-0.27
8								-0.26	-0.27	-0.27
9									-0.27	-0.27
10										-0.27

Table 1b Phase difference $(\theta_* - \Theta_T)$ expressed as fraction of wavelength
$\Gamma = 1$, $e = 0.01$, $a_T = 0.008$, $\Lambda_* = 4 \times 10^{-6}$, $\Lambda_T = 1.5 \times 10^{-6}$

m \ n	1	2	3	4	5	6	7	8	9	10
1	-0.25	-0.19	-0.16	-0.12	-0.03	0.11	0.19	0.22	0.23	0.24
2		-0.15	-0.12	-0.10	-0.04	0.19	0.29	0.32	0.33	0.33
3			-0.10	-0.08	-0.03	0.25	0.35	0.37	0.37	0.38
4				-0.06	-0.03	0.29	0.38	0.40	0.40	0.40
5					-0.02	0.33	0.40	0.41	0.42	0.42
6						0.35	0.42	0.43	0.43	0.43
7							0.45	0.44	0.44	0.44
8								0.456	0.45	0.45
9									0.45	0.45
10										0.46

Table 1c Phase difference $(\theta_* - \Theta_T)$ expressed as fraction of wavelength
$\Gamma = 1$, $e = 0.01$, $a = 0.008$, $\Lambda_* = 8 \times 10^{-6}$, $\Lambda_T = 3 \times 10^{-6}$

m \ n	1	2	3	4	5	6	7	8	9	10
1	-0.25	-0.14	-0.10	0.11	0.29	0.32	0.33	0.34	0.34	0.34
2		-0.09	-0.06	0.15	0.38	0.40	0.40	0.41	0.41	0.41
3			-0.04	0.17	0.42	0.42	0.43	0.44	0.44	0.44
4				0.17	0.44	0.45	0.45	0.45	0.45	0.45
5					0.45	0.46	0.46	0.46	0.46	0.46
6						0.46	0.47	0.47	0.47	0.47
7							0.47	0.47	0.47	0.47
8								0.48	0.48	0.48
9									0.48	0.48
10										0.48

Table 1d Phase difference $(\theta_* - \Theta_T)$ expressed as fraction of wavelength
$\Gamma = 1$, $e = 0.01$, $a_T = 0.008$, $\Lambda_* = 1.2 \times 10^{-5}$, $\Lambda_T = 4.5 \times 10^{-6}$

m \ n	1	2	3	4	5	6	7	8	9	10
1	-0.25	-0.11	-0.01	0.34	0.37	0.38	0.38	0.38	0.38	0.39
2		-0.06	-0.01	0.41	0.43	0.43	0.44	0.44	0.44	0.44
3			-0.00	0.44	0.45	0.45	0.46	0.46	0.46	0.46
4				-0.46	0.46	0.47	0.47	0.47	0.47	0.47
5					0.47	0.47	0.47	0.47	0.48	0.47
6						0.48	0.48	0.48	0.48	0.48
7							0.48	0.48	0.48	0.48
8								0.48	0.48	0.48
9									0.48	0.48
10										0.48

Table 1e Phase difference $(\theta_* - \Theta_T)$ expressed as fraction of wavelength
$\Gamma = 1$, $e = 0.01$, $a_T = 0.008$, $\Lambda_* = 2.4 \times 10^{-5}$, $\Lambda_T = 9 \times 10^{-6}$

m \ n	1	2	3	4	5	6	7	8	9	10
1	-0.25	-0.04	0.41	0.43	0.43	0.44	0.44	0.44	0.44	0.44
2		-0.02	0.45	0.46	0.47	0.47	0.47	0.47	0.47	0.47
3			0.47	0.48	0.48	0.48	0.48	0.48	0.48	0.48
4				0.48	0.48	0.48	0.48	0.48	0.48	0.48
5					0.48	0.49	0.49	0.49	0.49	0.49
6						0.49	0.49	0.49	0.49	0.49
7							0.49	0.49	0.49	0.49
8								0.49	0.49	0.49
9									0.49	0.49
10										0.49

Table 2a Relative amplitude of ψ_* and ψ_T
$\Gamma = 1$, $e = 0.01$, $a_T = 0.008$, $\Lambda_* = 0$, $\Lambda_T = 0$

m \ n	1	2	3	4	5	6	7	8	9	10
1	0.0275 0.6873	0.0777 0.6465	0.1416 0.5941	0.2083 0.5311	0.2690 0.4681	0.3190 0.4120	0.3574 0.3657	0.3852 0.3296	0.4041 0.3021	0.4160 0.2811
2		0.0259 0.43.12	0.0496 0.4138	0.0776 0.3898	0.1069 0.3604	0.1349 0.3282	0.1595 0.2958	0.1799 0.2656	0.1962 0.2391	0.2088 0.2166
3			0.0243 0.3037	0.0391 0.2938	0.0558 0.2803	0.0731 0.2638	0.0899 0.2450	0.1052 0.2253	0.1183 0.2059	0.1293 0.1878
4				0.0232 0.2319	0.0337 0.2251	0.0451 0.2162	0.0569 0.2052	0.0683 0.1928	0.0788 0.1795	0.0881 0.1662
5					0.0223 0.1865	0.0304 0.1813	0.0389 0.1747	0.0475 0.1667	0.0559 0.1577	0.0636 0.1480
6						0.0217 0.1554	0.0281 0.1511	0.0347 0.1458	0.0414 0.1395	0.0478 0.1326
7							0.0212 0.1327	0.0264 0.1290	0.0318 0.1246	0.0371 0.1195
8								0.0207 0.1154	0.0251 0.1122	0.0295 0.1084
9									0.0203 0.1018	0.0240 0.0989
10										0.0199 0.0908

Table 2b Relative amplitude of ψ_* and ψ_T
$\Gamma = 1$, $e = 0.01$, $a = 0.008$, $\Lambda_* = 4 \times 10^{-6}$, $\Lambda_T = 1.5 \times 10^{-6}$

m \ n	1	2	3	4	5	6	7	8	9	10
1	0.0110 0.2760	0.0382 0.2685	0.0928 0.2613	0.2171 0.2680	0.6957 0.3963	0.7140 0.3314	0.3326 0.1965	0.2197 0.1594	0.1649 0.1372	0.1316 0.1202
2		0.0115 0.1411	0.0303 0.1395	0.0757 0.1433	0.3083 0.2047	0.2863 0.1127	0.1240 0.0875	0.0838 0.0813	0.0647 0.0752	0.0530 0.0691
3			0.0169 0.0942	0.0433 0.0969	0.1879 0.1353	0.1680 0.0576	0.0725 0.0560	0.0495 0.0544	0.0386 0.0514	0.0319 0.0479
4				0.0302 0.0731	0.1345 0.1009	0.1185 0.0367	0.0512 0.0413	0.0351 0.0409	0.0274 0.0389	0.0228 0.0364
5					0.1049 0.0805	0.0917 0.0265	0.0396 0.0327	0.0272 0.0327	0.0213 0.0312	0.0178 0.0293
6						0.0750 0.0207	0.0324 0.0271	0.0223 0.0273	0.0175 0.0261	0.0146 0.0246
7							0.0275 0.0232	0.0189 0.0234	0.0128 0.0224	0.0124 0.0211
8								0.0164 0.0205	0.0129 0.0196	0.0108 0.0185
9									0.0114 0.0175	0.0095 0.0165
10										0.0085 0.0148

Table 2c Relative amplitude of ψ_* and ψ_T
$\Gamma = 1$, $e = 0.01$, $a_T = 0.008$, $\Lambda_* = 8 \times 10^{-6}$, $\Lambda_T = 3 \times 10^{-6}$

m \ n	1	2	3	4	5	6	7	8	9	10
1	0.0050 0.1253	0.0235 0.1266	0.0954 0.1409	0.5482 0.2015	0.1242 0.0918	0.0812 0.0875	0.0637 0.0824	0.0534 0.0768	0.0462 0.0711	0.0406 0.0655
2		0.0084 0.06412	0.0372 0.0711	0.2137 0.0512	0.0488 0.0418	0.0325 0.0427	0.0259 0.0413	0.0220 0.0391	0.0193 0.0367	0.0172 0.0343
3			0.0231 0.0474	0.1330 0.0229	0.0306 0.0273	0.0205 0.0283	0.0164 0.0275	0.0139 0.0262	0.0122 0.0247	0.0109 0.0231
4				0.0971 0.0130	0.0224 0.0204	0.0150 0.0212	0.0120 0.0206	0.0103 0.0197	0.0090 0.0185	0.0081 0.0174
5					0.0177 0.0162	0.0119 0.0169	0.0095 0.0165	0.0081 0.0157	0.0072 0.0148	0.0064 0.0139
6						0.0098 0.0141	0.0079 0.0138	0.0067 0.0131	0.0059 0.0124	0.0053 0.0116
7							0.0067 0.0118	0.0058 0.0112	0.0051 0.0106	0.0045 0.0100
8								0.0050 0.0098	0.0044 0.0093	0.0040 0.0087
9									0.0039 0.0083	0.0035 0.0078
10										0.0032 0.0070

Table 2d Relative amplitude of ψ_* and ψ_T
$\Gamma = 1$, $e = 0.01$, $a_T = 0.008$, $\Lambda_* = 1.2 \times 10^{-5}$, Λ_T 4.5×10^{-6}

m \ n	1	2	3	4	5	6	7	8	9	10
1	0.0032 0.0806	0.0216 0.0844	0.3747 0.2049	0.0754 0.0574	0.0462 0.0588	0.0365 0.0570	0.0312 0.0541	0.0275 0.0509	0.0246 0.0476	0.0222 0.0443
2		0.0087 0.04242	0.1795 0.1013	0.0329 0.0270	0.0201 0.0289	0.0161 0.0284	0.0138 0.0271	0.0123 0.0257	0.0110 0.0242	0.0100 0.0226
3			0.1182 0.0672	0.0209 0.0178	0.0130 0.1092	0.0104 0.0189	0.0090 0.0181	0.0086 0.0172	0.0072 0.0162	0.0065 0.0151
4				0.0155 0.0133	0.0097 0.0144	0.0077 0.0142	0.0067 0.0136	0.0059 0.0129	0.0053 0.0121	0.0049 0.0114
5					0.0077 0.0115	0.0062 0.0113	0.0053 0.0109	0.0047 0.0103	0.0043 0.0097	0.0039 0.0091
6						0.0051 0.0094	0.0044 0.0091	0.0039 0.0086	0.0035 0.0081	0.0032 0.0076
7							0.0038 0.0078	0.0034 0.0074	0.0030 0.0069	0.0028 0.0065
8								0.0020 0.0069	0.0027 0.0061	0.0029 0.0057
9									0.0024 0.0054	0.0021 0.0051
10										0.0019 0.0046

Table 2e Relative amplitude of ψ_* and ψ_T
$\Gamma = 1$, $e = 0.01$, $a_T = 0.008$, $\Lambda_* = 2.4 \times 10^{-5}$, $\Lambda_T = 9 \times 10^{-6}$

m \ n	1	2	3	4	5	6	7	8	9	10
1	0.0016 0.0389	0.0413 0.0521	0.10283 0.0281	0.0179 0.0298	0.0148 0.0293	0.0131 0.0281	0.0119 0.0267	0.0109 0.0252	0.0100 0.0237	0.0093 0.0222
2		0.0192 0.02602	0.0123 0.0138	0.0085 0.0149	0.0071 0.0146	0.0063 0.0140	0.0057 0.0134	0.0053 0.0126	0.0649 0.0110	0.0045 0.0111
3			0.0088 0.0092	0.0056 0.0099	0.0047 0.0097	0.0042 0.0094	0.0038 0.0089	0.0035 0.0084	0.0032 0.0079	0.0030 0.0074
4				0.0422 0.0074	0.0035 0.0073	0.0031 0.0070	0.0028 0.0067	0.0026 0.0063	0.0024 0.0059	0.0022 0.0056
5					0.0028 0.0058	0.0025 0.0056	0.0023 0.0053	0.0021 0.0051	0.0019 0.0048	0.0018 0.0045
6						0.0021 0.0047	0.0019 0.0045	0.0017 0.0042	0.0016 0.0040	0.0015 0.0037
7							0.0016 0.0038	0.0015 0.0036	0.0014 0.0034	0.0013 0.0032
8								0.0013 0.0032	0.0012 0.0030	0.0011 0.0028
9									0.0011 0.0026	0.0010 0.0025
10										0.0009 0.0022

Table 1a shows that for $\Lambda_* = \Lambda_T = 0$ the phase difference is always negative. For relative small values of Λ_* and Λ_T we see from Table 1b that the phase difference has turned positive for $n \geq 6$. For larger values (Table 1c and 1d) we find positive values for $n \geq 4$, while the largest values of Λ_* and Λ_T gives positive values for $n \geq 3$. (Table 1e). We notice also from these tables that $\theta_* - \theta_T = -0.25$ for $(m,n) = (1,1)$ and that when m and n are both large we gradually approach the value 0.5 for $\Theta_* - \Theta_T$. This is particularly so for the larger values of Λ_* and Λ_T.

So far we have used only the first equation in (2.10). The results in Table 1 may thus be considered as an extension of the study by Wiin-Nielsen (1961) to the spherical spectral domain. In the following we shall make use of both equations in the system (2.10). We may then solve for both the amplitudes and the absolute phase angles. Tables 2 a-e give the relative amplitudes for the mean flow and shear flow for the various pairs of Λ_* and Λ_T. Table 2a for $\Lambda_* = \Lambda_T = 0$ shows that the amplitude of ψ_* (the mean flow) for a fixed value of m is an increasing function of n, while the amplitude of ψ_T (the shear flow) is a decreasing function of n for a fixed value of m. This is radically changed for the other pairs of Λ_* and Λ_T. Table 2b shows that the maximum values of the two amplitudes are found close to the dividing line between negative and positive values of $(\Theta_*-\Theta_T)$. The corresponding observation can be made from Tables 2(c), (d) and (e). It is furthermore seen from these tables that the response decreases markedly as Λ_* and Λ_T increase. In view of these results it is clear that the response to the forcing ψ_E depends very much on whether or not the forcing field contains components with considerable amplitude close to the dividing line between positive and negative values of $(\Theta_*-\Theta_T)$.

The change in sign for $(\Theta_*-\Theta_T)$ in Tables 1b-e can be deduced from the solution given in (2.14). We note first that

$$\tan (m\,\Theta_T) = \frac{S}{Q} \text{ and } \tan (m\,\Theta_*) = \frac{(2-HG)S + (H+2G)Q}{(2-HG)Q - (H+2G)S} \tag{3.12}$$

From these formulas we find that

$$\tan [m(\Theta_*-\Theta_T)] = \frac{H+2G}{2-HG} \tag{3.13}$$

showing that $\Theta_*-\Theta_T = 0$ if $H+2G=0$. Using the definition of H and G in (2.11) we find that this condition is equivalent to

$$(2\frac{\Lambda_*}{\Omega} + \frac{\Lambda_T}{\Omega})(\frac{1}{2}C-1) = 2 \tag{3.14}$$

or

$$C = n(n+1) = 2\left[\frac{1}{\frac{\Lambda_*}{\Omega} + \frac{1}{2}\frac{\Lambda_T}{\Omega}} + 1\right] \tag{3.15}$$

(3.15) may be solved for n for given values of Λ_* and Λ_T. For the values used in Table 1 b-e we find:

Λ_*	Λ_T	n
2.0×10^{-6}	7.5×10^{-7}	7.48
4.0×10^{-6}	1.5×10^{-6}	5.06
8.0×10^{-6}	3.0×10^{-6}	3.69
1.2×10^{-5}	4.5×10^{-6}	3.03
2.4×10^{-5}	9.0×10^{-6}	2.21

These values of n are in agreement with Tables 1 b-e.

The next question is whether it is possible to explain the maxima which occur in Tables 2 b-e. It is well known that models of the present kind contain a resonance if the forcing and the dissipation are neglected. The resonance

will be determined in this case and compared with the maxima found in Tables 2 b-e. For this purpose we return to the system (2.10). Setting $e=a_T=\Gamma=0$ the system reduces to a homogeneous linear system. The following notation is introduced:

$$\ell_* = \frac{\Lambda_*}{\Omega}\ ,\ \ell_T = \frac{\Lambda_T}{\Omega},\ Z = \frac{1}{2}\,C-1,\ q = \frac{1}{2}\,\lambda^2 a^2 \tag{3.16}$$

The system will have non-trivial solutions if the determinant vanishes. This condition leads to the equation:

$$(\ell_* Z-1)(\ell_* Z-1 + \ell_* q) = \ell_T^2\ Z\ (Z-q) \tag{3.17}$$

(3.17) is a quadratic equation in Z for given values of Λ_* and Λ_T. It was solved for the pairs (Λ_*, Λ_T) used in Tables 2 b-e. The results are:

Λ_*	Λ_T	n
2.0×10^{-6}	7.5×10^{-7}	7.98
4.0×10^{-6}	1.5×10^{-6}	5.43
8.0×10^{-6}	3.0×10^{-6}	3.80
1.2×10^{-5}	4.5×10^{-6}	3.11
2.4×10^{-5}	9.0×10^{-6}	2.26

It is seen that these results compare favourably with the values given in Tables 2 b-e. The maxima occur for a fixed value of n in the tables and in the above approximate determinations. It may thus be concluded that the positions of the maxima in the response to the forcing can be determined rather well from the calculation of the resonance in the equations without forcing and dissipation.

4. THE VERTICAL SLOPE OF THE WAVES

In the previous section we have concentrated on the properties of the waves in the mean flow and the vertical shear flow. At several occasions we have indicated that when the wave in the vertical shear flow is lagging behind the wave in the mean flow the wave will slope from east to west in the vertical direction. This statement is normally true but there are exceptions because the vertical slope depends not only on the phase difference between the two waves, but also on their amplitude. It is thus necessary to investigate this question in details.

For this purpose it is most convenient to move the reference point for longitude to a point such that

$$\psi_* = A_* \cos(m \lambda) \tag{4.1}$$

The thermal wave may then be written in the form

$$\psi_T = A_T \cos (m \lambda + \Theta_T) \tag{4.2}$$

We shall assume that $0<\Theta_T<\pi$. This means that ψ_T is lagging behind ψ_*. For the waves at levels 1 and 3 in the two level model we obtain:

$$\psi_1 = \psi_* + \psi_T = (A_* + A_T \cos \theta_T) \cos(m \lambda) - A_T \sin \theta_T \sin (m \lambda)$$

$$\psi_3 = \psi_* + \psi_T = (A_* - A_T \cos \theta_T) \cos(m \lambda) + A_T \sin \theta_T \sin (m \lambda) \tag{4.3}$$

The phase angles for levels 1 and 3 may be calculated from (4.3). The same applies for the amplitudes.

With the definitions

$$\tan \Theta_1 = \frac{A_T \sin \Theta_T}{A_* + A_T \cos \Theta_T} \; ; \; \tan \Theta_3 = \frac{A_T \sin \Theta_T}{A_* - A_T \cos \Theta_T} \tag{4.4}$$

we find that

$$\psi_1 = [A_*^2 + A_T^2 + 2A_* A_T \cos \Theta_T]^{\frac{1}{2}} \cos(m\lambda + \Theta_1)$$

$$\psi_3 = [A_*^2 + A_T^2 - 2A_* A_T \cos \Theta_T]^{\frac{1}{2}} \cos(m\lambda - \Theta_3) \tag{4.5}$$

The maximum of ψ_1 is located at $-\Theta_1/m$ while the maximum of ψ_3 is found at Θ_3/m. It is seen from (4.4) that if $0<\Theta_T<\pi/2$ we have $\Theta_1>0$, and $\Theta_3>0$ if $A_*>A_T \cos \Theta_T$. On the other hand, if $\pi/2<\Theta_T<\pi$ we have $\Theta_3>0$, and $\Theta_1>0$ if $A_*>-A_T\cos \Theta_T$. Similarly, if the phase lag is less than a quarter of the wavelength the amplitude will increase with height, while it will decrease if $\pi/2<\Theta_T<\pi$.

To illustrate these relations it will suffice to calculate the two extreme cases, i.e. $\Lambda_* = 4.0 \times 10^{-6}$ s^{-1}, $\Lambda_T = 1.5 \times 10^{-6}$ s^{-1} and $\Lambda_* = 2.4 \times 10^{-5}$ s^{-1}, $\Lambda_T = 9.0 \times 10^{-6}$ s^{-1}. The relative amplitudes are reproduced in Tables 3a and 3b. We notice that the component (1,1) has the same amplitude at levels 1 and 3. This is due to the fact that for this component we have $\Theta_T = \pi/2$. A dashed line has been drawn in each table separating the region where $A_1>A_3$ from the one where $A_1<A_3$. It is seen that the long waves only have $A_1>A_3$. Table 3b shows the very small response obtained for the very large values of Λ_* and Λ_T.

Table 3a The amplitudes A_1 and A_3 for $\Lambda_* = 4 \times 10^{-6}s^{-1}$, $\Lambda_T = 1.5 \times 10^{-6}s^{-1}$

m \ n	1	2	3	4	5	6	7	8	9	10
1	0.28 0.28	0.28 0.26	0.32 0.23	0.45 0.18	1.09 0.32	1.00 0.51	0.44 0.32	0.29 0.25	0.23 0.20	0.18 0.17
2		0.15 0.13	0.16 0.12	0.21 0.09	0.51 0.12	0.34 0.27	0.13 0.17	0.09 0.14	0.09 0.12	0.06 0.11
3			0.11 0.08	0.14 0.06	0.32 0.16	0.18 0.18	0.18 0.11	0.06 0.09	0.04 0.08	0.03 0.07
4				0.10 0.05	0.23 0.04	0.12 0.13	0.04 0.09	0.02 0.07	0.02 0.06	0.02 0.06
5					0.19 0.03	0.08 0.11	0.02 0.07	0.02 0.06	0.02 0.05	0.02 0.05
6						0.07 0.09	0.02 0.06	0.01 0.05	0.01 0.04	0.01 0.04
7							0.01 0.05	0.01 0.04	0.01 0.04	0.01 0.03
8								0.01 0.04	0.01 0.03	0.01 0.03
9									0.01 0.03	0.01 0.03
10										0.01 0.02

Table 3b The amplitudes A_1 and A_3 for $\Lambda_* = 2.4 \times 10^{-5}\ s^{-1}$, $\Lambda_T = 9 \times 10^{-6}\ s^{-1}$

m \ n	1	2	3	4	5	6	7	8	9	10
1	0.04 0.04	0.09 0.02	0.02 0.05	0.02 0.05	0.02 0.04	0.02 0.04	0.02 0.04	0.02 0.04	0.01 0.03	0.01 0.03
2		0.05 0.01	0.004 0.03	0.01 0.02	0.01 0.02	0.01 0.02	0.01 0.02	0.01 0.02	0.01 0.02	0.01 0.02
3			0.002 0.02	0.004 0.02	0.005 0.01	0.005 0.01	0.005 0.01	0.005 0.01	0.005 0.01	0.004 0.01
4				0.003 0.01	0.004 0.01	0.004 0.01	0.004 0.01	0.004 0.01	0.004 0.01	0.003 0.01
5					0.003 0.009	0.003 0.008	0.003 0.008	0.003 0.007	0.003 0.007	0.003 0.006
6						0.003 0.007	0.003 0.006	0.003 0.006	0.002 0.006	0.002 0.005
7							0.002 0.005	0.002 0.005	0.002 0.005	0.002 0.004
8								0.002 0.004	0.002 0.004	0.002 0.004
9									0.002 0.004	0.002 0.004
10										0.001 0.003

Table 4a The phase angles θ_1 and θ_3 for $\Lambda_* = 4 \times 10^{-6}\ s^{-1}$, $\Lambda_T = 1.5 \times 10^{-6}\ s^{-1}$

m \ n	1	2	3	4	5	6	7	8	9	10
1	87.7 -87.7	61.2 -103.6	43.5 -102.1	24.0 -83.2	3.9 -13.6	-12.2 24.5	-24.3 35.1	-32.1 39.5	-36.8 42.7	-40.8 44.0
2		25.20 -61.02	17.9 -63.3	11.86 -57.8	2.9 -12.4	-8.9 11.6	-19.8 15.1	-28.1 15.9	-33.3 16.6	-36.6 17.5
3			10.2 -45.7	6.7 -43.9	1.5 -8.2	-6.3 6.3	-16.3 7.8	-24.3 8.2	-28.3 9.0	-31.8 8.7
4				3.8 -36.1	1.2 -7.0	-4.5 3.8	-13.3 4.8	-21.3 4.8	-25.0 5.3	-26.8 5.6
5					0.6 -4.4	-3.3 2.5	-11.1 3.2	-18.3 3.6	-22.4 3.4	-23.8 3.6
6						-2.5 1.8	-9.4 2.2	-17.0 2.3	-19.8 2.5	-21.0 2.6
7							-8.1 1.6	-15.5 1.7	-18.0 1.9	-19.0 2.0
8								-14.5 1.2	-16.7 1.4	-17.5 1.4
9									-14.9 1.2	-15.6 1.3
10										-14.8 0.9

Table 4b The phase angles Θ_1 and Θ_3 for $\Lambda_* = 2.4 \times 10^{-5} s^{-1}$, $\Lambda_T = 9 \times 10^{-6} s^{-1}$

m \ n	1	2	3	4	5	6	7	8	9	10
1	87.6 -87.6	8.8 -125.3	-73.1 16.1	-125.5 15.8	-133.2 16.8	-141.5 14.8	-142.7 15.0	-143.5 15.1	-144.1 15.2	-144.2 15.3
2		2.1 -76.9	-43.2 4.6	-74.0 4.6	-79.7 3.6	-80.3 3.7	-80.7 3.8	-80.8 3.8	-80.9 3.8	-81.0 3.8
3			-32.6 1.8	-54.5 1.5	-55.4 1.6	-55.7 1.7	-55.8 1.7	-55.9 1.7	-56.0 1.7	-56.0 1.7
4				-40.9 1.1	-41.6 1.2	-41.8 1.2	-41.9 1.3	-41.9 1.3	-42.0 1.3	-42.0 1.3
5					-33.2 1.0	-34.7 0.5	-34.8 0.5	-34.8 0.5	-34.8 0.5	-34.8 0.5
6						-28.9 0.4	-29.0 0.4	-29.0 0.4	-29.0 0.4	-29.0 0.4
7							-24.8 0.4	-24.8 0.4	-24.8 0.4	-24.8 0.4
8								-21.7 0.3	-21.8 0.3	-21.8 0.3
9									-19.3 0.3	-19.3 0.3
10										-17.4 0.3

Tables 4a and 4b contain the phase angles θ_1 and θ_3. In each table a dashed line has been introduced to separate the eastward and westward sloping components. These dashed lines agree with the separations in Table 1b and 1e between the waves in the mean flow and the shear flow. The unit in Table 4a,b is degrees, and the value indicate the position of the maximum (the ridge). The long waves have a slope which in some cases approaches a half wave length. Similarly, the westward sloping waves have also for large values of m and n a slope coming close to half a wavelength. The slope is of course smallest close to the dividing line.

We may thus conclude that when the very long stationary waves slope westward with height in the winter and eastward in the summer it is due to the seasonal change in the zonal wind which is strong during the winter season and weak during the summer season. A comparison with data studies available so far is difficult because they are based on Fourier analysis along longitude circles, and the slope is thus given as a function of m only.

The energetics of the long term stationary waves in the model will be investigated in this section. As usual we distinguish between eddy available potential energy and eddy kinetic energy. The energy generations, transformations and dissipations are well known for the two level model. In the present model we may have generation of eddy available potential energy G(A'), conversion from zonal to eddy available potential energy $C(\bar{A},A')$,

conversion from eddy available potential energy to eddy kinetic energy C(A',K') and dissipation of the eddy kinetic energy D(K'). The formulas for the calculations are:

$$
\begin{aligned}
G(A') &= \frac{2P}{g}\,\lambda^2\,\gamma\,\frac{1}{S}\int_S \psi_T'\,(\psi_E' - \psi_T')\,dS \\
C(\bar{A},A') &= \frac{2P}{g}\,\lambda^2\,\Lambda_T\,\frac{1}{S}\int_S \psi_T'\,\frac{\partial\psi_*'}{\partial\lambda}\,dS \\
C(A',K') &= \frac{2P}{g}\,\frac{1}{S}\int_S \frac{f_o}{P}\,\omega\psi_T'\,dS \\
D(K') &= \frac{2P}{g}\left\{\frac{\varepsilon}{2}\,\frac{1}{S}\int_S (\psi_*'-\psi_T')(\nabla^2\psi'-2\nabla^2\psi')dS + A\,\frac{1}{S}\int_S \psi_T'\nabla^2\psi_T'\right\}
\end{aligned}
\tag{4.6}
$$

In view of the stationarity of the waves it is obvious that C(A',K') = D(K') and that G(A') + C($\bar{A}$, A') = C(A', K'). D(K') is presumably positive although no guarantee can be given. It is thus most interesting to calculate G(A') and C($\bar{A}$,A'). For each separate wave we get

$$
\begin{aligned}
\frac{1}{A_E^2}\,G(A') &= \frac{2P}{g}\;\Gamma\;a^2\Omega^3\;\left(\frac{A_T}{A_E}\right)\left(\cos m\,\theta_T - \frac{A_T}{A_E}\right) \\
\frac{1}{A_E^2}\,C(\bar{A},A') &= \frac{2P}{g}\;\left(\tfrac{1}{2}\lambda^2a^2\right)\left(a^2\Omega^2\right)\;m\;\Lambda_T\left(\frac{A_*}{A_E}\right)\left(\frac{A_T}{A_E}\right)\;\sin[m(\theta_*-\theta_T]
\end{aligned}
\tag{4.7}
$$

where the associated Legendre functions are normalised such that

$$
\frac{1}{2}\int_{-1}^{+1} P_n^m(\mu)^2\,d\mu = 1 \tag{4.8}
$$

It is seen that G(A') is positive when

$$
\cos(m\,\theta_T) > \frac{A_T}{A_E} \tag{4.9}
$$

Table 5 $A_E^{-2} x G(A')$ and $A_E^{-2} x C(\bar{A}, A')$ for $\Lambda_* = 4 \times 10^{-6} s^{-1}$, $\Lambda_T = 1.5 \times 10^{-6} s^{-1}$.

m \ n	1	2	3	4	5	6	7	8	9	10
1	3.49 -1.53	9.20 -4.36	15.64 -8.44	22.29 -14.47	24.22 -15.81	-10.12 37.61	4.13 15.67	8.08 8.45	9.18 5.24	9.26 3.50
2		3.04 -1.49	5.54 -3.00	8.67 -5.73	12.57 -10.10	-10.38 24.04	1.12 7.58	3.45 4.10	4.25 2.61	4.50 1.79
3			2.66 -1.44	4.28 -2.84	6.77 -5.68	-6.18 13.36	0.50 3.99	1.79 2.18	2.27 1.41	2.44 0.98
4				2.50 -1.66	4.10 -3.49	-3.86 8.17	0.28 2.40	1.07 1.32	1.37 0.86	1.49 0.60
5					2.72 -2.33	-2.60 5.44	0.18 1.58	0.71 0.87	0.91 0.57	0.99 0.40
6						-1.85 3.86	0.13 1.12	0.50 0.62	0.65 0.40	0.71 0.29
7							0.09 0.83	0.37 0.46	0.48 0.30	0.53 0.21
8								0.29 0.35	0.37 0.23	0.41 0.16
9									0.29 0.18	0.32 0.13
10										0.26 0.11

Table 6 $A_E^{-2} \times G(A')$ and $A_E^{-2} \times C(\bar{A}, A')$ for $\Lambda_* = 8\ x_T 10^{-6} s^{-1}$, $\Lambda_T = 3 \times 10^{-6} s^{-1}$.

m \ n	1	2	3	4	5	6	7	8	9	10
1	0.98 -0.61	3.10 -2.13	7.69 -6.38	-51.66 67.75	-3.28 8.92	0.73 4.73	2.39 3.11	3.25 2.21	3.69 1.63	3.87 1.23
2		0.83 -0.57	2.17 -1.81	-14.53 18.28	-0.91 2.37	0.18 1.31	0.67 0.89	0.95 0.65	1.11 0.50	1.20 0.39
3			0.99 -0.83	-6.47 8.07	-0.41 1.06	0.08 0.59	0.31 0.41	0.44 0.30	0.52 0.23	0.56 0.18
4				-3.63 4.52	-0.23 0.60	0.05 0.34	0.17 0.23	0.25 0.17	0.29 0.13	0.32 0.10
5					-0.15 0.38	0.03 0.22	0.11 0.15	0.16 0.11	0.19 0.08	0.21 0.07
6						0.02 0.15	0.08 0.10	0.11 0.08	0.13 0.06	0.14 0.05
7							0.06 0.08	0.08 0.06	0.10 0.04	0.11 0.03
8								0.06 0.04	0.07 0.03	0.08 0.03
9									0.06 0.03	0.06 0.02
10										0.05 0.02

Inspecting the table of θ_T (not reproduced here) it is found that (4.9) is satisfied except in a narrow region close to, but not identical to the region in which $\theta_*-\theta_T$ changes sign. $C(\bar{A},A')$ is negative when the wave is sloping from west to east with increasing height. This happens in the model for sufficiently small values of n. To illustrate these points Tables 5 and 6 have been prepared. They contain the quantities $A_E^{-2}\ G(A')$ and $A_E^{-2}\ C(\bar{A},A')$. Table 5 is calculated for small values of Λ_* and Λ_T resulting in a change of sign for $C(\bar{A},A')$ between n=5 and n=6. $G(A')$ is positive everywhere except for n=6. However, the sum of $G(A')$ and $C(\bar{A},A')$ is positive everywhere and equal to the dissipation of eddy kinetic energy. Table 6 contains the results for $\Lambda_* = 8 \times 10^{-6}s^{-1}$ and $\Lambda_T = 3 \times 10^{-6}s^{-1}$. In this case $C(\bar{A},A')$ changes sign between n=3 and n=4 while $G(A')$ is negative for n=4 and n=5. The sum of $G(A')$ and $C(\bar{A},A')$ is again positive everywhere.

The sum of the numbers in the two tables is equal to $C(A',K')$. It is seen that $C(A',K')$ has a maximum at n=6 in Table 5 and n=4 in Table 6. These scales represent therefore the maximum input in the spectrum of the kinetic energy.

5. A STUDY OF CLIMATOLOGICAL MAPS

As pointed out in Sect.4 it is difficult to verify the present results using previous studies because the decomposition usually is made in Fourier components along selected latitude circles. It was therefore decided to make a study of the climatological maps prepared by the National Center for Atmospheric Research (NCAR). These maps are used as climatological maps although they are averages based on about 15 years of data. Although the maps are global, the present study has used the Northern Hemisphere only because a contrast between winter and summer is needed in the zonal flow.

A decomposition of the height fields in spherical harmonic functions was made for 100, 85, 70, 50 and 30 cb under the assumption that the fields are symmetrical around the equator. In terms of the indices m and n in the associated Legendre polynomials this restricts the elements to those for which m+n is even. The complex coefficients were converted to an amplitude and a phase angle using the previous conventions except that the phase indicates the position of the first ridge, i.e. an element is

$$A(m,n) \cos [m\lambda-\theta] P_n^m(\mu) \tag{5.1}$$

The decomposition was made for the months of January and July to obtain a strong contrast. These months will be described separately. The truncation was in each case $m \leq n$, $m \leq 10$, $n \leq 10$.

We present first the results for the phase angle for July. Since the theory presented in the previous section of this paper indicates that the important parameter is n we shall arrange the results of the data study in a similar way.

Fig.1 shows the vertical slope of the waves with n=1 and 2. They slope toward the east with height. The slopes for n=3 and 4 are shown in Fig.2 in which the element (1,3) slopes from east to west, while (2,4) and (4,4) slope the other way. (3,3) is not shown in the figure because it represents only 0.3% of the total kinetic energy showing that the amplitude is small which in turn means that the determination of amplitude and phase are very uncertain. A similar decision has been made in the other figures. The component (1,3) is not a major component in the two-dimensional spectrum because it contains only 1.7% of the eddy kinetic energy, and of this amount almost 90% comes from the 30 cb contribution. The amplitudes at the other levels are therefore very small giving uncertainty in the phase determination. On the other hand, the components with n=3 are close to those components which could be excited by the influence of the mountains because the meridional half wavelength for n=3 is about 3300 km which corresponds roughly to the width of the mountain ranges (Charney and Eliassen, 1949; Wiin-Nielsen, 1961). Fig.3 shows the results for n=5 and 6. It is seen that the waves with n=5 slope from west to east, while those with n=6 have a westward slope with height. Fig.4 for n=7 and 8 shows the same tilt as n=6. We have thus arrived at the conclusion that apart from the low-energy wave (1,3) all waves with $n \leq 5$ slope toward east with height while the opposite slope exists for $n \geq 6$. The July climatological map confirms therefore the theory developed in this paper.

If the theory is correct we should also expect for the month of January that a larger number of waves will show a westward tilt. The following figures will confirm that this is so. Fig.5 contains the tilt curves for January for n=1,2,3 and 4, Fig.6 for n=5 and 6, and Fig.7 for n=7 and 8. All curves show a westward slope. The theory predicts that the single component (1,1) should

always be to the east at variance with Fig.5 but this discrepancy between theory and observation is due to the simplified theory in which the zonal flow contribution cancels exactly for n=1 (C=2) and only for this value.

As described earlier we have used the contribution from a given component to the eddy kinetic energy as a criterion to determine if the phase angle is reliably determined. A by-product of this procedure is the eddy kinetic energy spectrum for n=1 to 10. If ψ is the streamfunction we may write the kinetic energy in the form

$$K = \frac{1}{g}\frac{1}{4\pi}\int_{o}^{p_o}\int_{-1}^{+1}\int_{o}^{2\pi}(-\frac{1}{2}\psi\ \nabla^2\psi)d\lambda\ d\mu\ dp \tag{5.2}$$

Let ψ be represented by the series

$$\psi = \sum_{n=1}^{10}\sum_{m\leq n}^{10} B(m,n)\ P_n^m(\mu)\ \cos\ (m\lambda-\sigma) \tag{5.3}$$

It follows that

$$\nabla^2\psi = -\frac{n(n+1)}{a^2}\psi \tag{5.4}$$

Having 5 levels in the vertical direction we may write

$$K = \sum_{i=1}^{5}\{\frac{\Delta p_i}{g}\frac{1}{8a^2}\sum_{m,n} n(n+1)\ B(m,n)^2\} \tag{5.5}$$

The spherical harmonic coefficients A(m,n) obtained from the height field are available. We use the most simple assumption

$$\psi = \frac{g}{f_o}Z;\quad B(m,n) = \frac{g}{f_o}A(m,n) \tag{5.6}$$

for the evaluation and obtain

$$K = \sum_{i=1}^{5}\sum_{m,n} L_i\ n(n+1)\ A(m,n)^2 \tag{5.7}$$

where

$$L_i = \frac{\Delta p_i \; g}{8a^2 \; f_o^2} \tag{5.8}$$

Fig.8 shows the two spectra for January and July as a function of n. Maxima occur at n=5 and n=7 in January and n=5 and n=9 in July.

It is finally of interest to calculate an average angular velocity for the January and July climatological maps. $\Lambda(\mu)$ may be obtained geostrophically from the formula

$$\Lambda(\mu) = - \frac{g}{f_o a^2} \frac{d\bar{Z}}{d\mu} \tag{5.9}$$

in which $\bar{Z}(\mu)$ is the average height along a latitude circle. The average value of Λ is then

$$\bar{\Lambda} = \int_o^1 \Lambda \, d\mu = - \frac{g}{f_o a^2} \left(\bar{Z}(1) - \bar{Z}(0)\right) \tag{5.10}$$

$\bar{Z}(1)$ and $\bar{Z}(0)$ may be calculated from the spherical harmonic coefficients, i.e.

$$\bar{Z}(1) = \sum_m A_n P_n(1) = A_o + \sqrt{5} A_2 + 3A_4 + \sqrt{13} A_6 + \sqrt{17} A_8 + \sqrt{21} A_{10} \tag{5.11}$$

because the unnormalized value of the associated Legendre polynomial is 1. Finally,

$$\bar{Z}(0) = \sum_m A_n P_n(0) = A_o - \frac{1}{2}\sqrt{5} A_2 + \frac{1}{4} \cdot \frac{3}{2} \cdot 3A_4 - \frac{1}{8} \cdot \frac{3.5}{2.3} \sqrt{13} A_6 + \frac{1}{16} \frac{3.5.7}{2.3.4} \sqrt{17} A_8 - \frac{1}{32} \cdot \frac{3.5.7.9}{2.3.4.5} \sqrt{21} \, A_{10} \tag{5.12}$$

Using these formulas we find

January: $\Lambda_* = 3.0 \times 10^{-6} \; s^{-1}$; $\Lambda_T = 1.8 \times 10^{-6} \; s^{-1}$

July: $\Lambda_* = 1.5 \times 10^{-6} \; s^{-1}$; $\Lambda_T = 0.5 \times 10^{-6} \; s^{-1}$

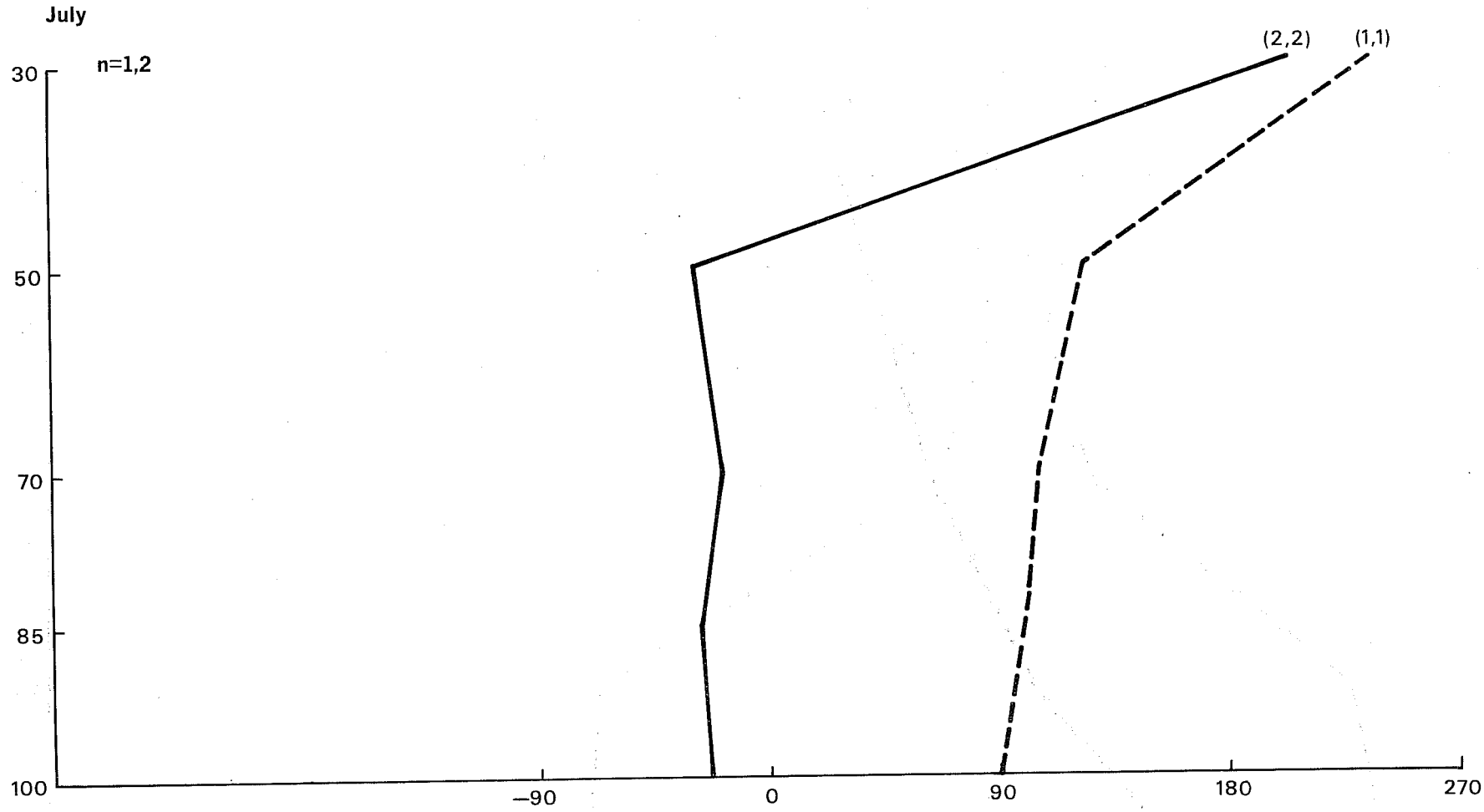

Fig. 1 : Vertical slope of the spherical harmonic elements (1,1) and (2,2) based on the climatological maps for July. Abscissa in deg. long and ordinate in cb.

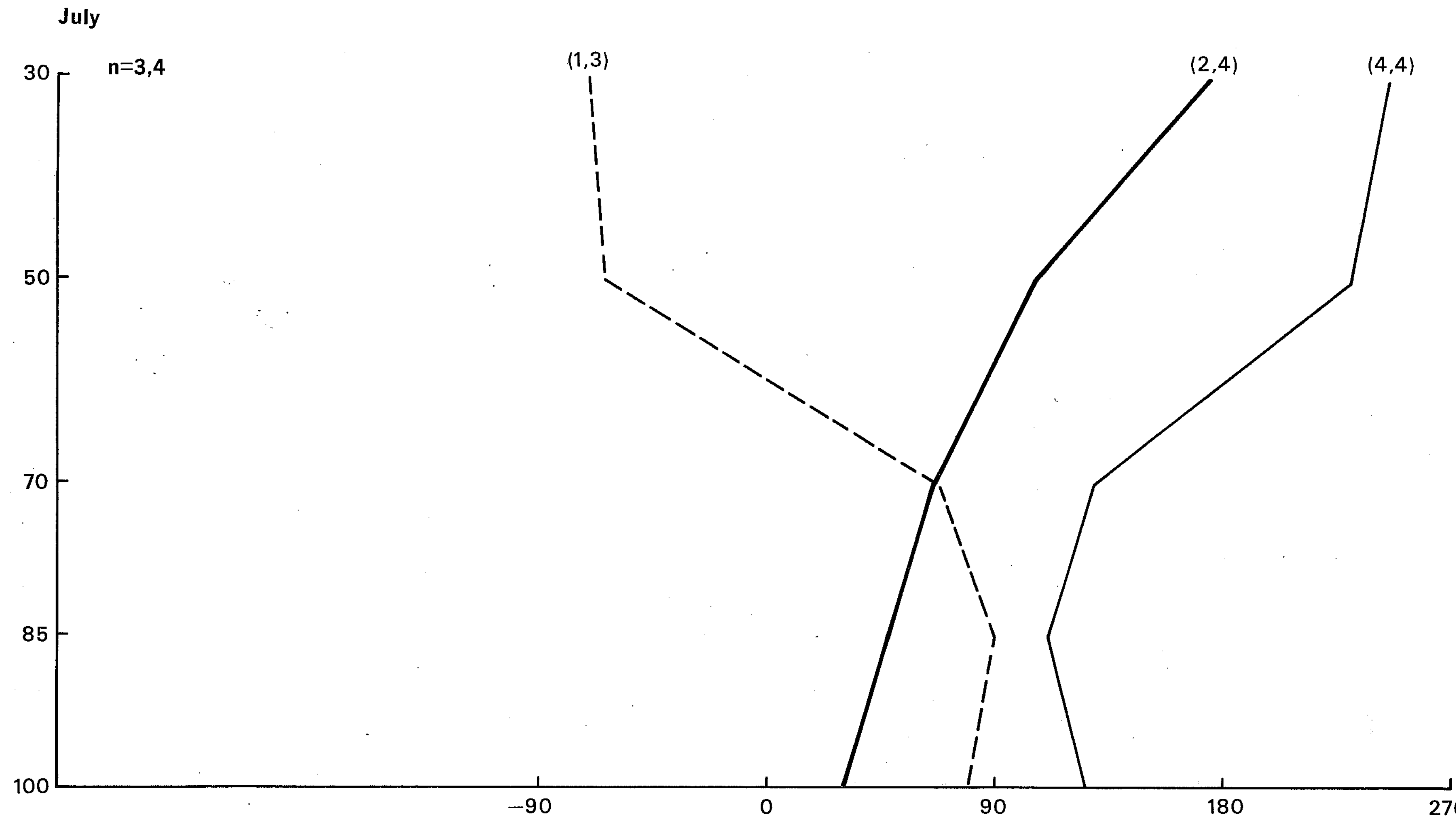

Fig. 2 : Vertical slope of the elements (1,3) (2,4) and (4,4) for July.

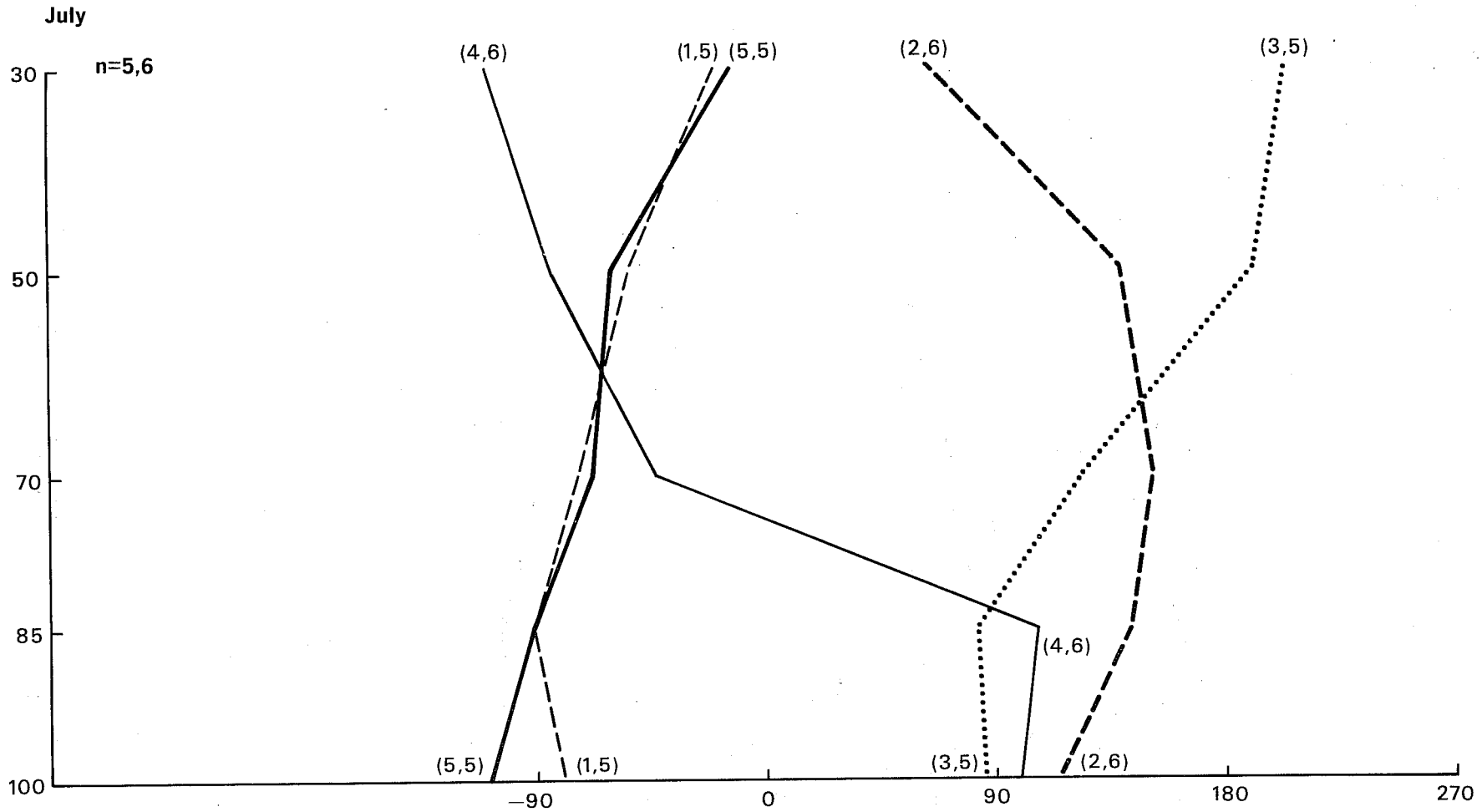

Fig. 3 : Vertical slope of the elements (1,5) (3,5) (5,5) (2,6) and (4,6) for July.

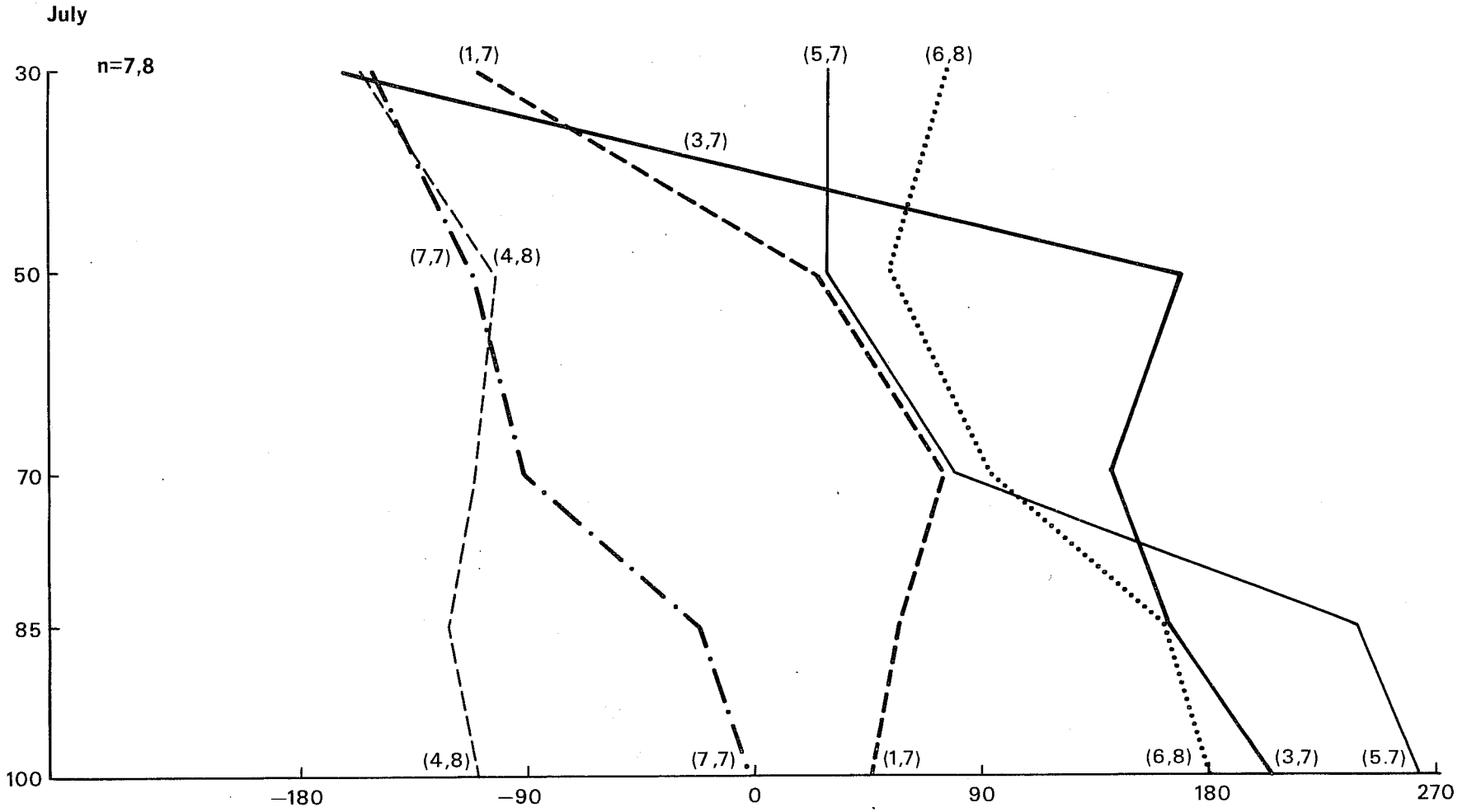

Fig. 4 : Vertical slope of the elements (1,7) (3,7) (5,7) (7,7) and (6,8) for July.

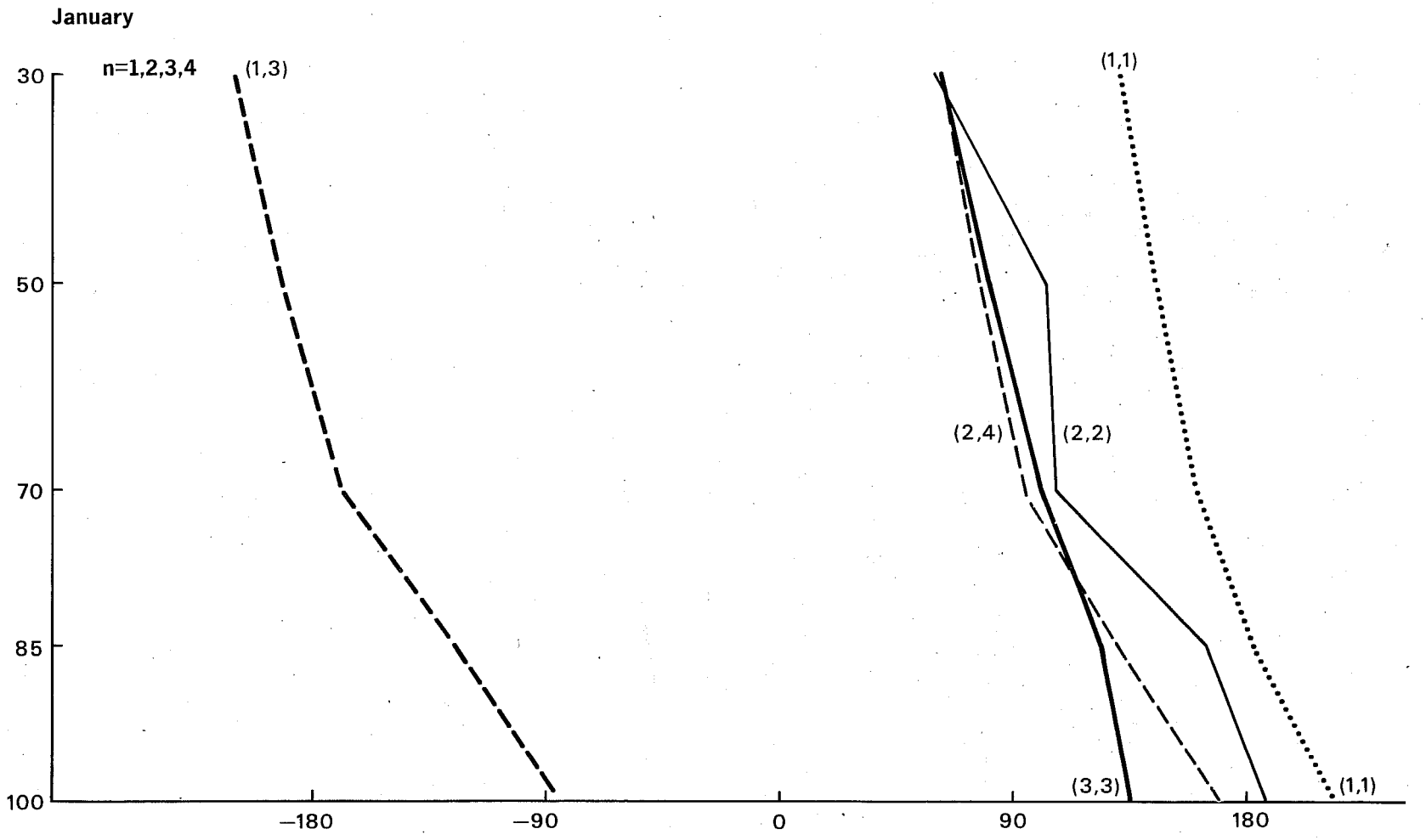

Fig. 5 : Vertical slope of the elements (1,1) (2,2) (2,4) (1,3) and (3,3) for January.

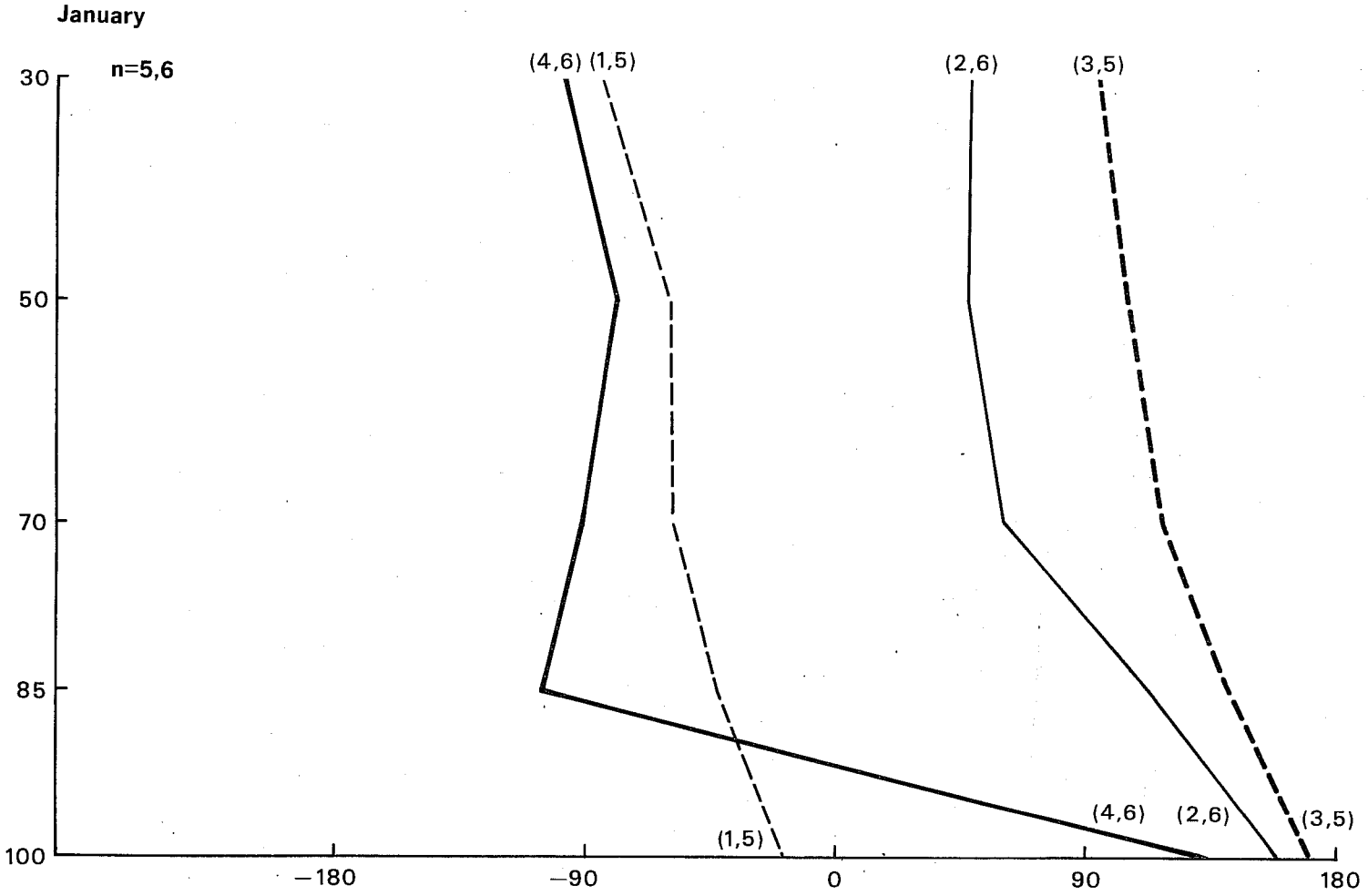

Fig. 6 : Vertical slope of the elements (1,5) (3,5) (2,6) and (4,6) for January.

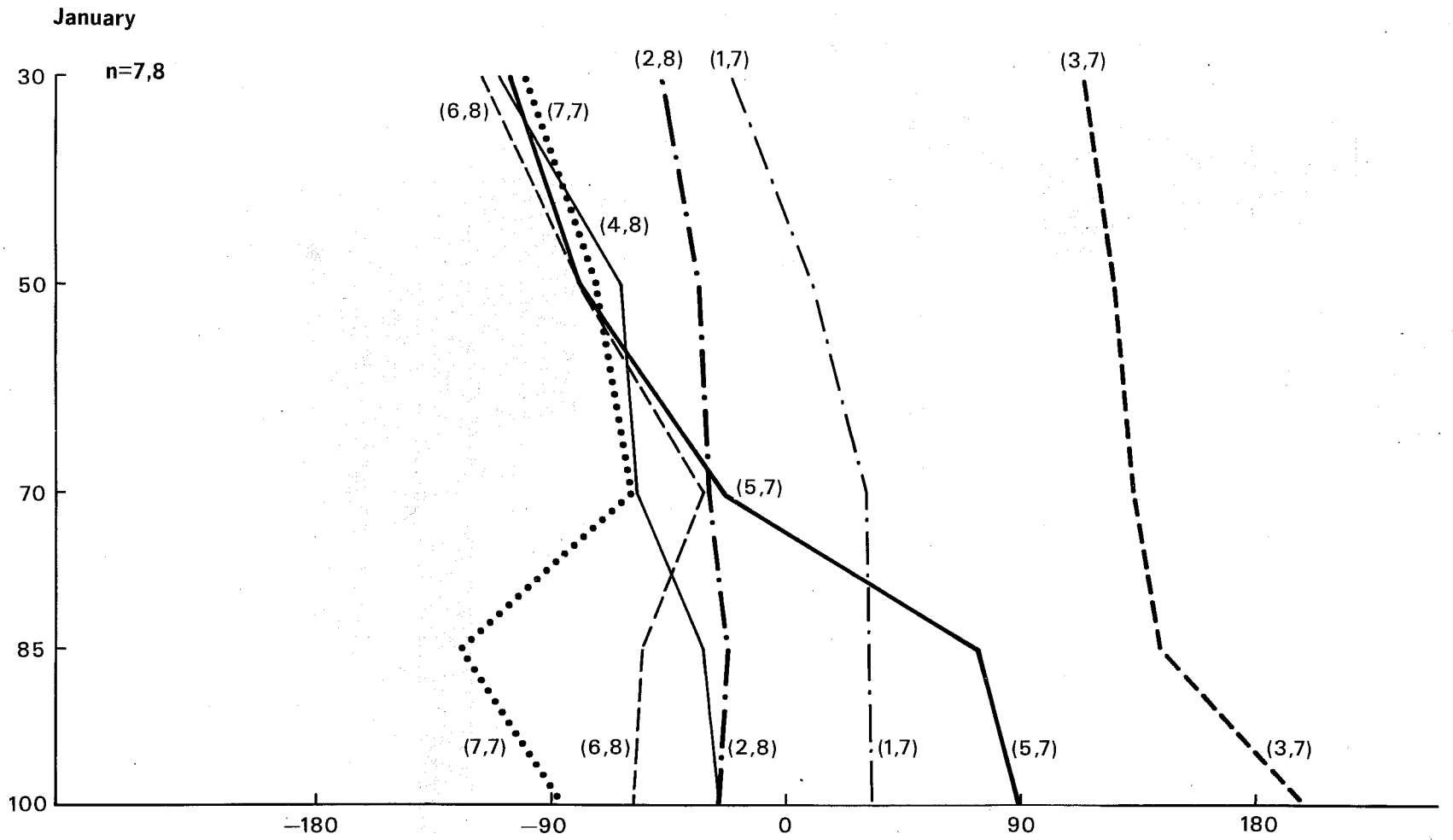

Fig. 7 : Vertical slope of the elements (1,7) (3,7) (5,7) (7,7) (2,8) (4,8) and (6,8) for January.

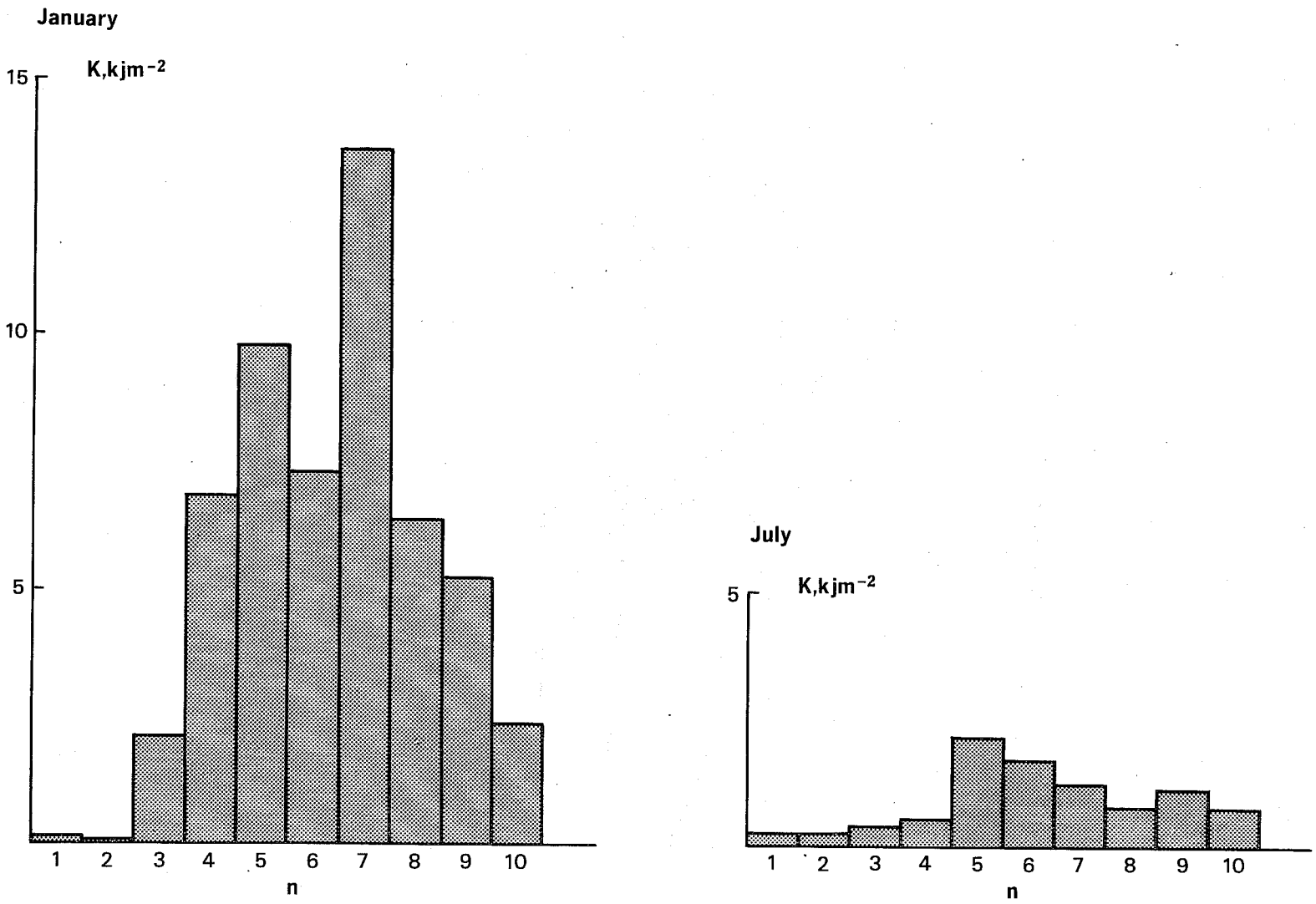

Fig. 8 : Kinetic energy spectra in KJm^{-2} computed geostrophically from climatological maps for January and July as a function of the meridional index (n).

6. STATIONARY WAVES FORCED BY OROGRAPHY

There is general agreement that the stationary long waves are forced by the effects of mountains and heating (Charney and Eliassen, 1949; Smagorinsky, 1953; Derome and Wiin-Nielsen, 1971). The mountain effect has not been included in the present studies so far. In this section we shall consider this effect in isolation thus neglecting the heat sources using once again the same model. The standard way to incorporate the mountain effect is by considering the forced vertical velocity which is

$$\omega_m \cong -g\rho_o w_m = - g\rho_o \underline{V}_m \cdot \nabla h = - g \frac{p_o}{RT_o} \underline{V}_m \cdot \nabla h \tag{6.1}$$

when the subscript m refers to the mountains. In the vorticity equation ω_m appears in the form:

$$\frac{f_o}{2P} \omega_m = - \frac{gf_o}{RT_o} (\Lambda_* - 2 \Lambda_T) \frac{\partial h}{\partial \lambda} \tag{6.2}$$

h will be scaled using the height H of the homogeneous atmosphere, i.e.

$$H = \frac{p_o}{g\rho_o} = \frac{RT_o}{g} \tag{6.3}$$

Let T(m,n) be the spherical harmonic coefficients corresponding to h/H. Considering further the scaling used in deriving (2.10) we find that this system is replaced by:

$$\begin{aligned} (1 + iG)\, A_* - (2 - iH)\, A_T &= i \frac{1}{2} \frac{m}{eC} \left(\frac{\Lambda_*}{\Omega} - 2 \frac{\Lambda_T}{\Omega}\right) T(m,n) \\ - (1 - iK)\, A_* + (M + iL)\, A_T &= i \frac{1}{2} \frac{m}{eC} \left(\frac{\Lambda_*}{\Omega} - 2 \frac{\Lambda_T}{\Omega}\right) T(m,n) \end{aligned} \tag{6.4}$$

where the notation is identical to the one used in Sect.2. From (6.4) it is straightforward, but laborious to calculate $A_*/T(m,n)$ and $A_T/T(m,n)$ in terms of an amplitude and a phase. In this section we have adopted the trigonometric part in the form $\cos(m\lambda-\theta)$. We shall be interested mainly in the phase angle. It is shown in Tables 7a and 7b for two different cases.

Table 7a Phase angles θ_* and θ_T for $\Lambda_* = 2\times10^{-6}s^{-1}$, $\Lambda_T = 7.5\times10^{-7}s^{-1}$

m \ n	1	2	3	4	5	6	7	8	9	10
1	-172.03 1.51	-154.82 1.94	-116.41 2.26	-62.51 -10.94	-35.15 -19.41	-22.03 -24.62	-13.39 -26.50	-6.00 -25.63	1.61 -22.13	10.43 -15.39
2		-168.93 1.08	-158.80 -1.10	-144.21 -7.79	-117.92 -18.74	-54.71 -28.62	0.92 -30.38	23.49 -20.00	36.26 1.40	45.13 23.28
3			-167.00 -0.73	-160.61 -5.75	-154.10 -16.26	-147.12 -30.51	30.66 -37.06	39.55 -20.81	43.95 11.26	47.45 30.11
4				-166.47 -4.50	-163.52 -13.79	-164.54 -30.18	-214.33 -43.04	49.56 -23.20	44.94 15.49	45.04 29.88
5					-167.74 -11.77	-169.72 -28.76	-196.82 -47.88	56.26 -26.10	43.67 17.03	41.62 27.87
6						-172.20 -26.92	-191.78 -51.67	60.98 -29.12	41.55 17.25	38.15 25.53
7							-189.27 -54.60	64.44 -32.08	39.17 16.83	34.95 23.29
8								67.06 -34.91	36.79 16.13	32.06 21.28
9									34.51 15.32	29.53 19.51
10										27.28 17.96

Table 7b Phase angles θ_* and θ_T for $\Lambda_* = 8\times10^{-6}s^{-1}$, $\Lambda_T = 3\times10^{-6}s^{-1}$

m \ n	1	2	3	4	5	6	7	8	9	10
1	180.40 182.91	180.58 188.54	176.62 199.48	43.87 -30.13	21.95 7.33	22.23 14.30	24.41 18.43	27.00 21.44	29.64 23.79	32.13 25.69
2		180.29 184.28	178.31 189.84	27.59 -17.61	11.68 3.86	11.76 7.44	12.94 9.59	14.38 11.17	15.87 12.42	17.31 13.44
3			178.88 186.57	19.50 -12.16	7.88 2.60	7.92 5.00	8.73 6.44	9.71 7.51	10.73 8.35	11.72 9.04
4				14.95 -9.23	5.94 1.96	5.97 3.76	6.57 4.84	7.32 5.65	8.09 6.28	8.84 6.80
5					4.76 1.57	4.78 3.01	5.27 3.88	5.87 4.52	6.49 5.03	7.09 5.45
6						3.99 2.51	4.39 3.24	4.89 3.77	5.41 4.20	5.92 4.54
7							3.77 2.77	4.20 3.24	4.64 3.60	5.08 3.90
8								3.68 2.83	4.06 3.15	4.44 3.41
9									3.61 2.80	3.95 3.03
10										3.56 2.73

Table 7a, corresponding to weak zonal winds, shows a behaviour of the spherical harmonics similar to a corresponding table using heat forcing. The largest scales contain waves in which z_* is lagging behind z_T, i.e. eastward slope with height. The change takes place at n=5,6 for m=1, at n=6,7 for m=2,3 and at n=7,8 for the remaining part of Table 7a as shown by the dashed curve.

Table 7b indicates that the dividing line is between n=3 and n=4. It is furthermore seen that the numerical values of the differences $\theta_*-\theta_T$ are much smaller in this case. $\theta_T-\theta_T$ is particularly small for large values of the meridional scale parameter n.

An inspection of additional calculations for other values of Λ_* and Λ_T indicates that the change in sign for $\theta_*-\theta_T$ occurs in agreement with the values of n computed from (3.17) which indicates those meridional scales for which resonance would take place in the case of flow without forcing and dissipation. In view of the qualitative similarity between forcing by heating and mountains in this respect we shall not pursue the forcing by topography any further in this section.

7. THE TRANSIENT WAVES

The previous sections described a study of the stationary fields in the atmosphere as forced by heating and mountains. For each spherical harmonic element we may consider that it consists of two parts, the stationary and the transient parts of which the stationary part may be obtained by a time-average over a sufficiently long time. The climatological maps used in Sect.5 are averages over an ensemble of data sets, each of which represents a given period such as a month. It is believed that a climatological map is a reasonable representation of the stationary field. The transient state is the difference between the total state and a representation of the stationary state. This concept may be used on any meteorological parameter or on a spherical harmonic element.

Although the calculations in the previous sections have been done with a triangular truncation T-10 it is not believed that these elements are stationary. We have tried to describe the stationary part using linear analysis. In this section we shall investigate the transient part using a model which includes heating and friction. A very large number of stability studies of baroclinic flows are available in the meteorological literature, and it is hardly possible to find anything new in this kind of investigation. However, the literature does not seem to contain the necessary information in the form needed here.

Studies on the beta plane of the influence of friction on baroclinic stability was first carried out by Holopainen (1961) and by Haltiner and Caverly (1965), while Wiin-Nielsen et al. (1967) and Haltiner (1967) investigated the influence of various aspects of heating and friction. Baroclinic stability studies in the case of adiabatic and frictionless flow using a spherical geometry were performed by Hollingsworth (1975) and Hollingsworth, Simmons and

Hoskins (1976). In this section we shall include perturbation heating and friction in the most simple, two level, quasi-geostrophic model. This is of course equivalent to adding time-dependence to the model used in Sect.2. The perturbation equations are those used in (2.4). Dropping the primes we have

$$\frac{\partial \nabla^2\psi_*}{\partial t} + \Lambda_* \frac{\partial \nabla^2\psi_*}{\partial \lambda} + \Lambda_T \frac{\partial \nabla^2\psi_T}{\partial \lambda} + \frac{2(\Omega+\Lambda_*)}{a^2}\frac{\partial \psi_*}{\partial \lambda} + \frac{2\Lambda_T}{a^2}\frac{\partial \psi_T}{\partial \lambda} = -\frac{1}{2}\varepsilon(\nabla^2\psi_* - 2\nabla^2\psi_T) \tag{7.1}$$

$$\frac{\partial [\nabla^2\psi_T - \lambda^2\psi_T]}{\partial t} + \Lambda_* \frac{\partial [\nabla^2\psi_T - \lambda^2\psi_T]}{\partial \lambda} + \Lambda_T \frac{\partial (\nabla^2\psi_* - \lambda^2\psi_*)}{\partial \lambda} + \frac{2(\Omega+\Lambda_*)}{a^2}\frac{\partial \psi_T}{\partial \lambda} + \frac{2\Lambda_T}{a^2}\frac{\partial \psi_*}{\partial \lambda}$$

$$= \lambda^2 \gamma \psi_T - 2A\nabla^2\psi_T + \frac{1}{2}\varepsilon(\nabla^2\psi_* - 2\nabla^2\psi_T) \tag{7.2}$$

We adopt the same scaling as in Sect.2 and seek solutions of the form (2.8) except that time-dependence is added in the exponential function using

$$\exp[im(\lambda - st)]$$

where s is the phase speed. Following standard procedure we derive two homogeneous linear equations for the complex amplitudes A_* and A_T. They are:

$$\left\{s - \Lambda_* + \frac{2(\Omega+\Lambda_*)}{C} + i\frac{\varepsilon}{2m}\right\} A_* - \left\{\frac{C-2}{C}\Lambda_T + i\frac{\varepsilon}{m}\right\} A_T = 0 \tag{7.3}$$

$$\left\{\frac{r-C+2}{r+C}\Lambda_T - i\frac{\varepsilon C}{2m(r+C)}\right\} A_* + \left\{s - \Lambda_* + \frac{2(\Omega+\Lambda_*)}{r+C} + i\frac{1}{m(r+C)}(\gamma r + 2AC + \varepsilon C)\right\} A_T = 0 \tag{7.4}$$

in which $C = n(n+1)$ and $r = \lambda^2 a^2$. We notice that the heating and the dissipation appear in the imaginary parts of the coefficients to A_* and A_T. The adiabatic and non-viscous case in thus obtained by disregarding these imaginary components. It is seen from (7.4) that the heating in the present Newtonian form acts qualitatively in the same way as the dissipation although the dissipation is more strongly scale-dependent than the heating due to the factor C. If (7.3) and (7.4) shall have non-trivial solutions the determinant must vanish. Denoting $Z = s - \Lambda_*$ this condition results in a second degree equation with complex coefficients. It is:

$$Z^2 + (E + iF)Z + (G + iH) = 0 \tag{7.5}$$

where

$$E = \frac{2C+r}{C(r+C)} \cdot 2(\Omega+\Lambda_*)$$

$$F = \frac{\varepsilon(r+3C) + 2\gamma r + 4AC}{2m\ (r+C)} \tag{7.6}$$

$$G = \frac{4(\Omega+\Lambda_*)^2}{C(r+C)} - \Lambda_T^2 \cdot \frac{(C-2)(C-r-2)}{C(r+C)} - \frac{\varepsilon}{2m^2} \frac{(\gamma r + 2AC)}{r+C}$$

$$H = \frac{2\gamma r + 3\varepsilon C+4AC}{mC(r+C)} (\Omega + \Lambda_*) + \frac{\varepsilon(2r-3C+6)}{2m(r+C)} \Lambda_T$$

The case of adiabatic and frictionless conditions is easily obtained from (7.5) and (7.6) by setting $\varepsilon = A = \gamma = o$. This condition leads to $F = H = 0$ and disregarding the last term in G. The solution is then:

$$Z = -\frac{2C+r}{C(r+C)} (\Omega+\Lambda_*) \pm \left\{(\Omega+\Lambda_*)^2 \frac{r^2}{C^2(r+C)^2} - \Lambda_T^2 \frac{(C-2)(2+r-C)}{C(r+C)}\right\}^{\frac{1}{2}} \tag{7.7}$$

As expected instability will occur for sufficiently large values of Λ_T provided $2+r>C$. The solution is stable for all values of Λ_T when $C=n(n+1)<2+r$ which leads to $n<9.68$. The critical windshear $\Lambda_{T,cr}$ needed for instability is

$$\Lambda_{T,cr} = (\Omega+\Lambda_*) \frac{r}{[C(C-2)(C+r)(2+r-C)]^{\frac{1}{2}}} \tag{7.8}$$

$\Lambda_{T,cr}$ as a function of n is shown in Fig.9 for $\Lambda_* = o$, showing that the minimum value occurs at n=8. The e-folding time is

$$T_e = \frac{1}{mC_i} \tag{7.9}$$

and is shown in Fig.10 for $\Lambda_* = 8 \times 10^{-6}\ s^{-1}$, $\Lambda_T = 3 \times 10^{-6}\ s^{-1}$ and expressed in days.

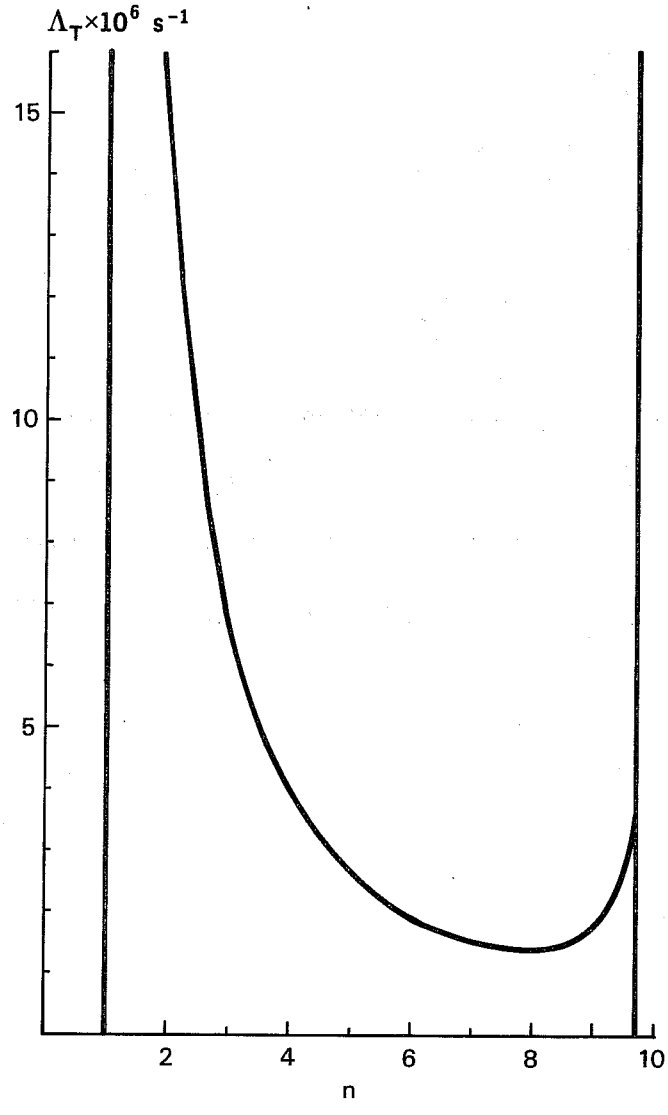

Fig. 9 : Critical windshear in the unit $10^6 5^{-1}$ necessary for instability as a function of the meridional index (n). Adiabatic, frictionless case.

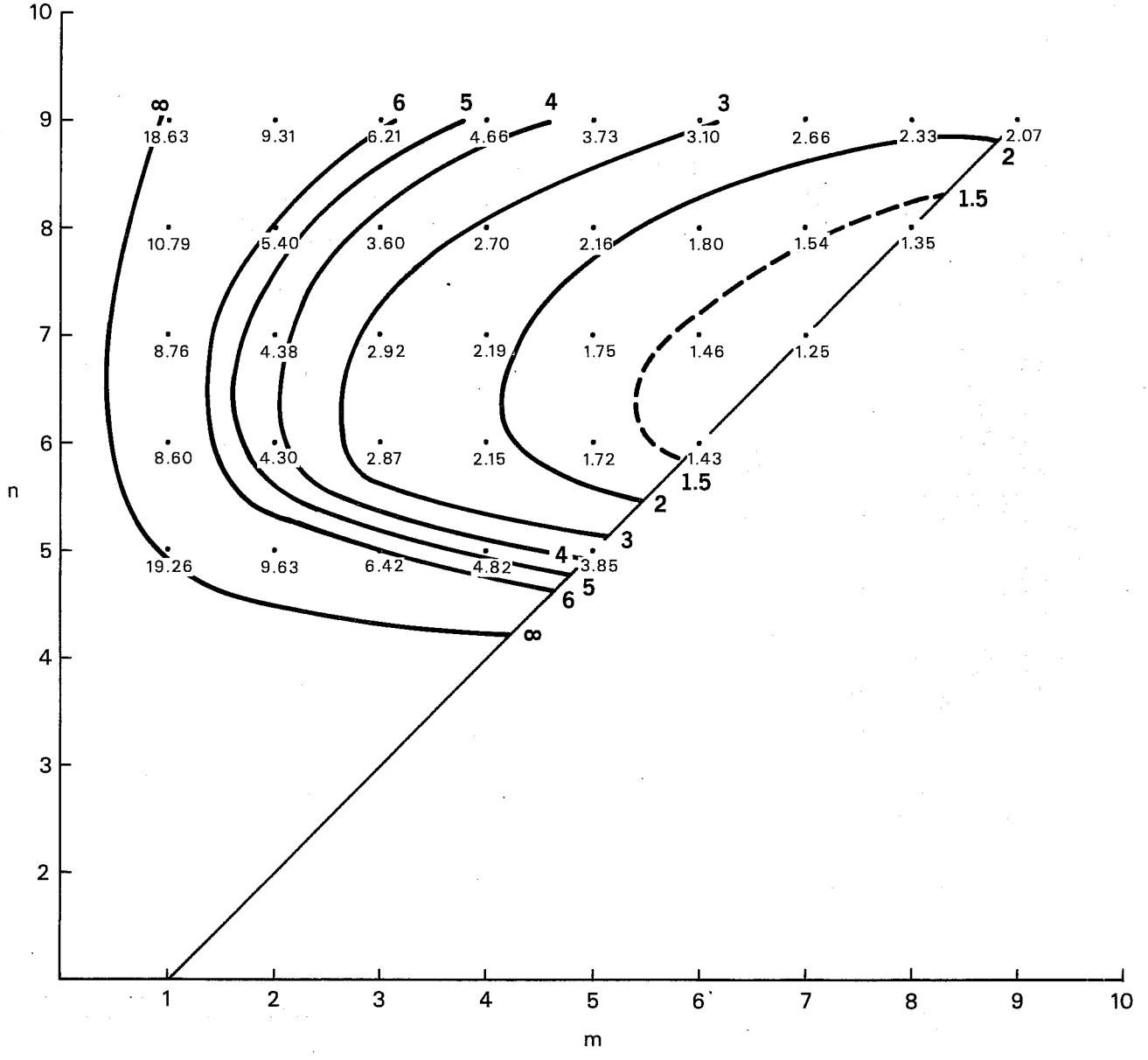

Fig. 10 : The e-folding time measured in days, for the adiabatic, frictionless case as a function of m and n. Parameters : $\Lambda_* = 8 \times 10^{-6}\ s^{-1}$, $\Lambda_T = 3 \times 10^{-6}\ s^{-1}$.

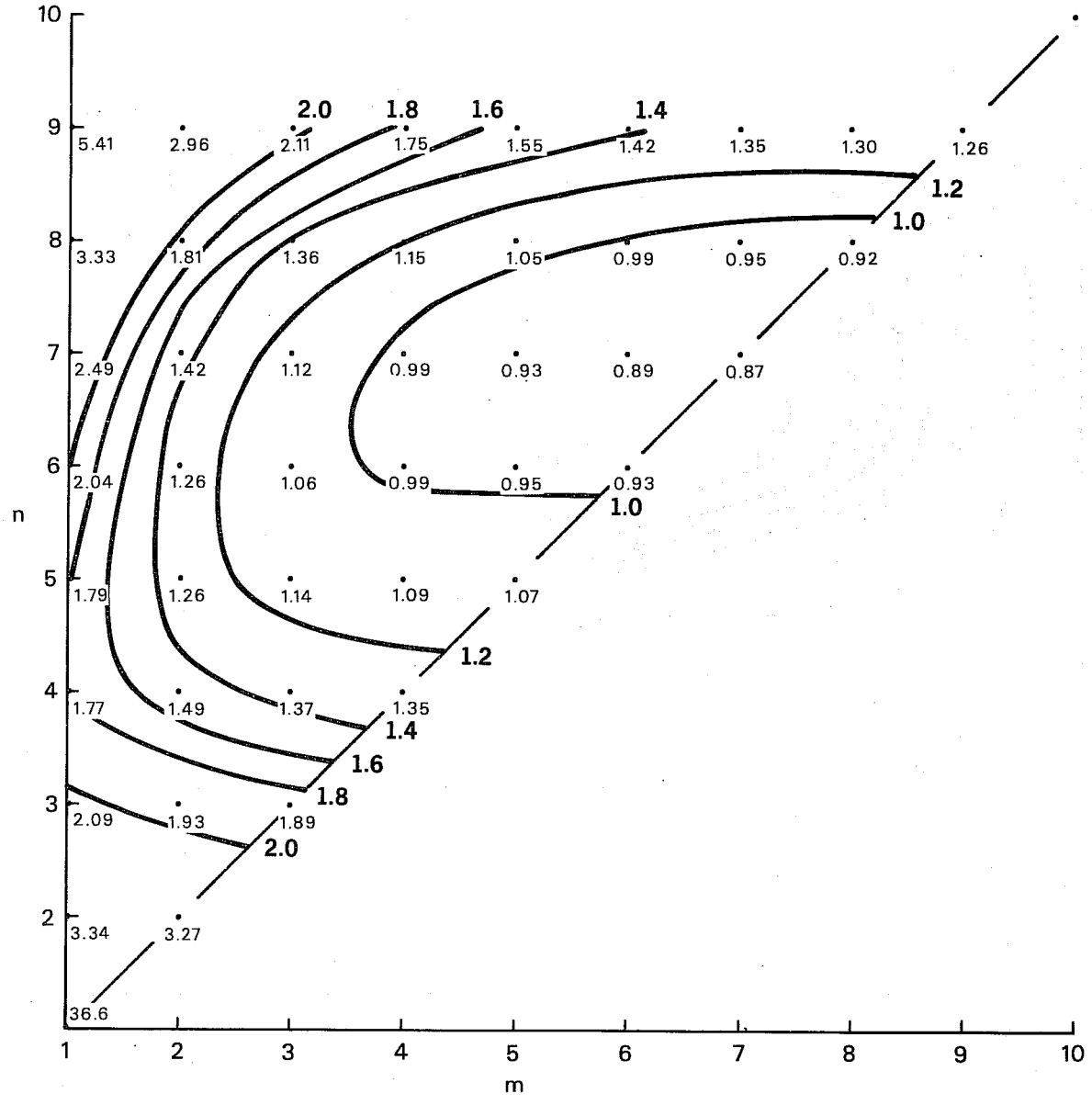

Fig. 11 : The critical windshear, measured in $10^6 s^{-1}$, necessary for instability ($\Lambda_* = 0$) as a function of m and n.

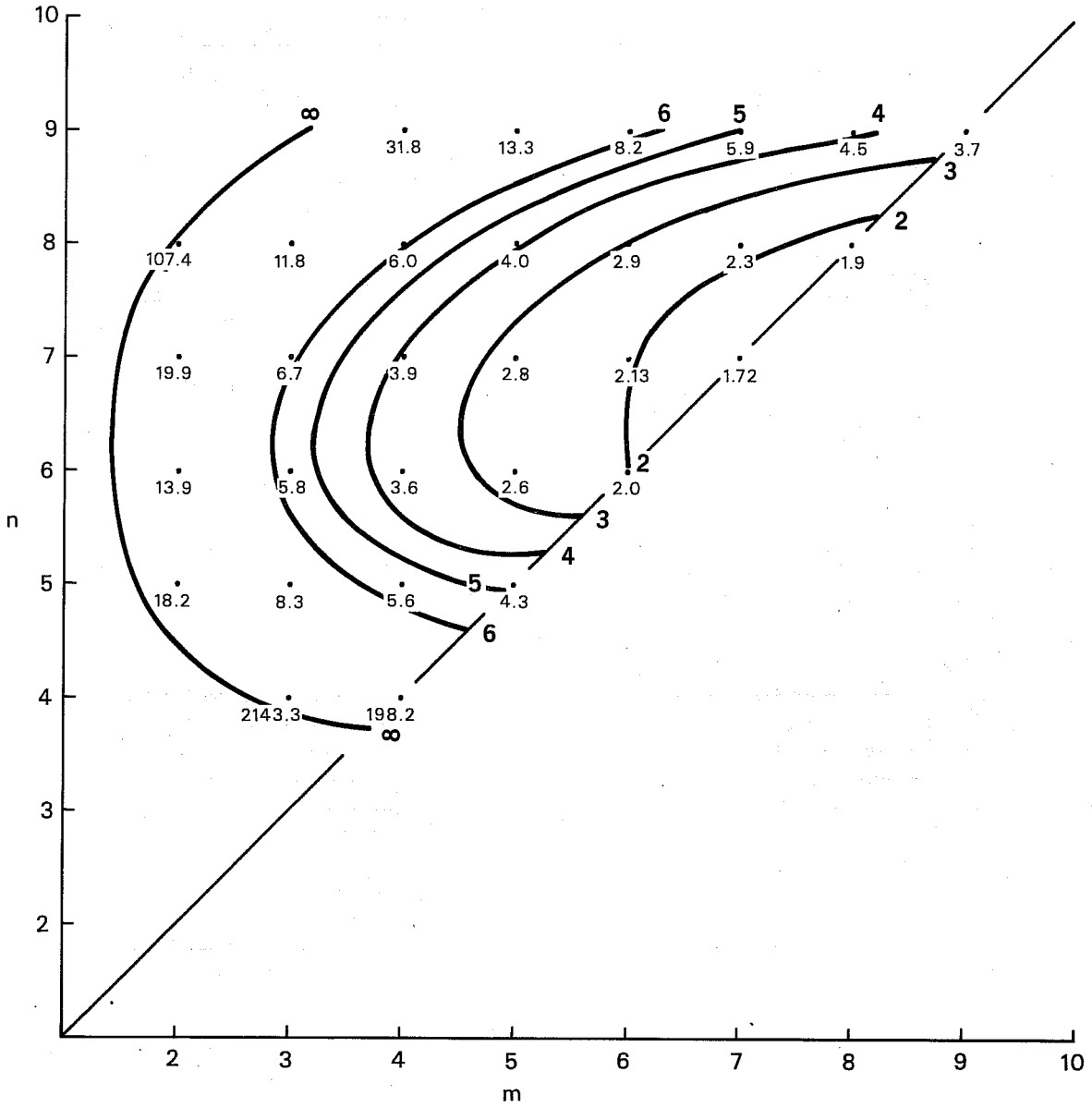

Fig. 12 : The e-folding time, measured in days, for $\Lambda_* = 8 \times 10^{-2} s^{-1}$ and $\Lambda_T = 3 \times 10^{-6} s^{-1}$ as a function of m and n.

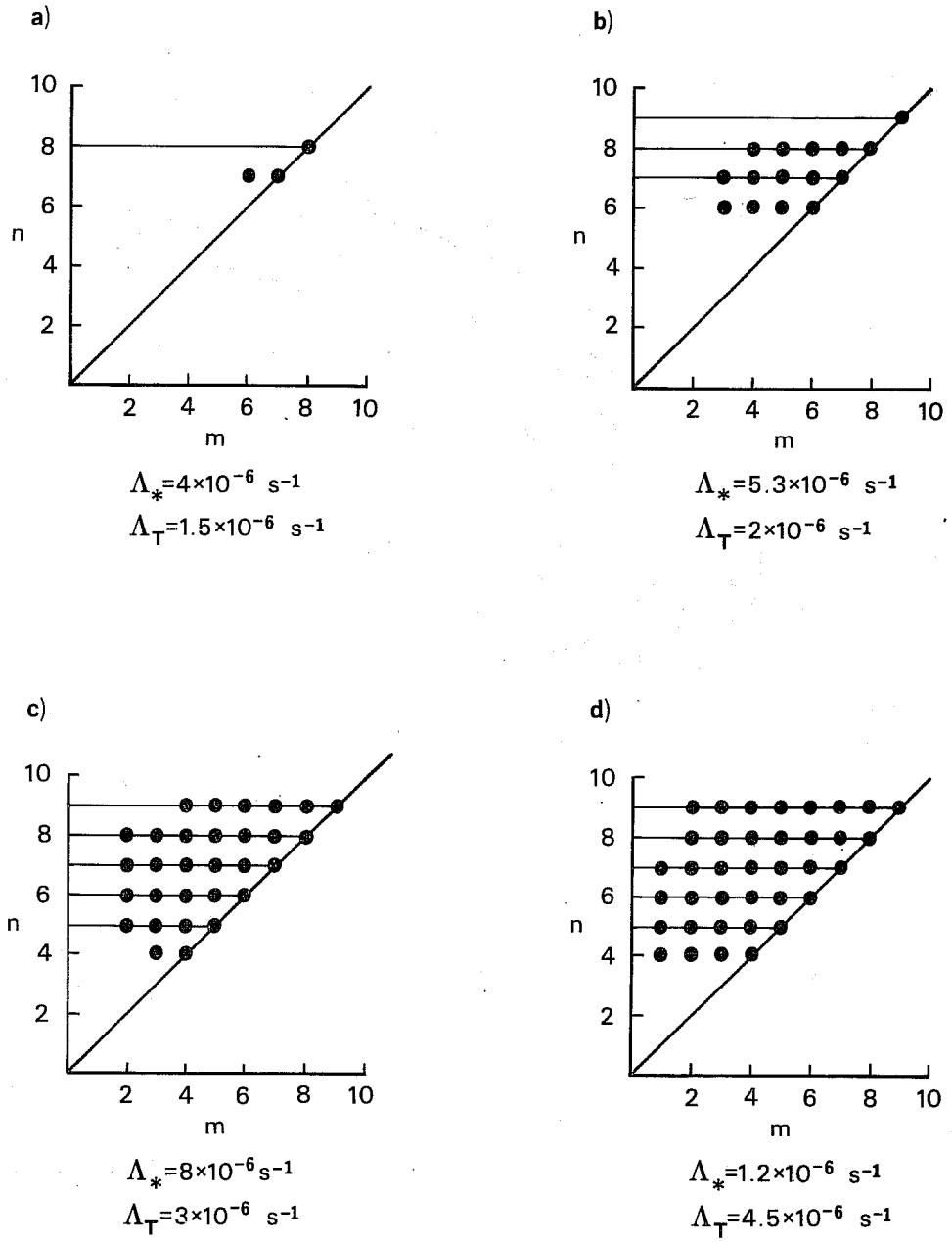

Fig. 13 : Schematic illustration of the influence of heating and friction on baroclinic instability. The horizontal lines indicate the values of n for which instability exists in the adiabatic and frictionless case. Dots indicate elements which are unstable when heating and friction are included.

We return now to the general case for which (7.5) and (7.6) apply. The solution of (7.5) may be written in the form:

$$Z = \begin{cases} \frac{1}{2}\left[-E+\left\{\frac{(K^2+L^2)^{\frac{1}{2}}+K}{2}\right\}^{\frac{1}{2}} + i\left\{\left(\frac{(K^2+L^2)^{\frac{1}{2}}-K}{2}\right)^{\frac{1}{2}} - F\right\}\right] \\ \frac{1}{2}\left[-E-\left\{\frac{(K^2+L^2)^{\frac{1}{2}}+K}{2}\right\}^{\frac{1}{2}} - i\left\{\left(\frac{(K^2+L^2)^{\frac{1}{2}}-K}{2}\right)^{\frac{1}{2}} + F\right\}\right] \end{cases} \tag{7.10}$$

in which

$$K = E^2 - F^2 - 4G; \quad L = 2(EF-2H) \tag{7.11}$$

Instability occurs when $Z(i)>0$. Since $F>o$ according to (7.6) it follows that the second root in (7.10) corresponds to stability. However, the first root may give instability if

$$[(K^2 + L^2)^{\frac{1}{2}} - K]^{\frac{1}{2}} > F\sqrt{2} \tag{7.12}$$

Using the definitions in (7.11) we may rewrite (7.12) in the form

$$GF^2 + H^2 - EFH>0 \tag{7.13}$$

We notice that G has a term containing Λ_T^2 while H has a term containing Λ_T. It is thus possible to write the expression in (7.13) as a second degree polynomial in Λ_T. This expression may be used to determine the critical value of Λ_T necessary for instability. The results are shown in Fig.11 for $\Lambda_*=0$. The critical windshear is now a function of both m and n. A comparison between Fig.9 and Fig.11 shows that a smaller critical windshear is needed to create instability when heating and friction is added. However, a better measure is to consider the e-folding time which is shown in Fig.12 which should be compared with Fig.10. It is seen that the general effect of heating and friction is to increase the e-folding time and thus to make the flow less unstable. As a final comparison we consider Fig.13 in which we have compared

the spherical harmonic elements which are stable and unstable in the two cases. In each figure, characterized by given values of Λ_* and Λ_T, the horizontal straight lines indicate those values of n for which instability exists in the adiabatic and frictionless cases, while the dots indicate those elements which are unstable when heating and friction are included. For example, in Fig.13(a) there is such a small windshear that only n=8 is unstable in the first case. In the second only three elements (6,7), (7,7) and (8,8) are unstable. All parts of Fig.13 show that the inclusion of heating and friction has the effect of stabilizing some large scale components and, in addition, of destabilizing some components for lower values of n.

The analysis described above was not made to provide still another stability study of a two-level, quasi-geostrophic model, but rather to provide the information needed to study the structure of the waves. We consider first the phase angle difference between the waves in the mean flow and the shear flow. For this purpose we can use either (7.3) or (7.4). Solving (7.3) for A_T and assuming that $A_* = A_*(r)$ we find after some reductions that $\tan \theta_T =$

$$\frac{\frac{C-2}{C}\Lambda_T\left(s(i)+\frac{\varepsilon}{2m}\right)-\frac{\varepsilon}{m}\left(s(r)-\Lambda_*+\frac{2(\Omega+\Lambda_*)}{C}\right)}{\frac{C-2}{C}\Lambda_T\left(s(r)-\Lambda_*+\frac{2(\Omega+\Lambda_*)}{C}\right)+\frac{\varepsilon}{m}\left(s(i)+\frac{\varepsilon}{2m}\right)} \qquad (7.14)$$

where θ_T is the phase difference.

It is convenient at this time to compute a measure of the transport of sensible heat by the baroclinic wave. The integral

$$H_T = \frac{1}{2\pi}\int_0^{2\pi}\left(\eta_T\frac{\partial\tilde{\eta}_*}{\partial\lambda}+\tilde{\eta}_T\frac{\partial\eta_*}{\partial\lambda}\right)d\lambda \qquad (7.15)$$

is proportional to the heat transport. A tilde in (7.15) means the complete conjugate of a complex number. Evaluation of (7.15) leads to

$$H_T = e^{2msit} \left[P_n^m(\mu)\right]^2 \text{ im } (A_* \tilde{A}_T - \tilde{A}_* A_T) \tag{7.16}$$

Inserting from (7.3) in (7.15) we obtain

$$H_T = e^{2msit} (P_n^m)^2 \frac{2m A_* \tilde{A}_*}{(\frac{C-2}{2} \Lambda_T)^2 + (\frac{\varepsilon}{m})^2} \left\{\frac{C-2}{C} \Lambda_T \left(s(i) + \frac{\varepsilon}{2m}\right) - \frac{\varepsilon}{m} \left(s(r) - \Lambda_* + \frac{2(\Omega+\Lambda_*)}{c}\right)\right\} \tag{7.17}$$

It is easy to show that the denominator in (7.14) is positive for the unstable wave for which $s(i)>0$. The requirement is that the expression in the first term of the denominator is positive. From the upper expression in (7.10) which applies to the unstable case we get

$$s(r) - \Lambda_* + \frac{2(\Omega+\Lambda_*)}{C} = \frac{1}{2\sqrt{2}} \left[(K^2+L^2)^{\frac{1}{2}} + K\right]^{\frac{1}{2}} + \frac{r(\Omega+\Lambda_*)}{C(r+C)} > 0 \tag{7.18}$$

A comparison between (7.14) and (7.17) shows therefore that if $\theta_T>0$, then $H_T>0$. Considering first the adiabatic and non-viscous case we find from (7.14) that

$$\tan \theta_T = \frac{s(i)}{s(r) - \Lambda_* + \frac{2(\Omega+\Lambda_*)}{C}} \tag{7.19}$$

θ_T is thus positive for the unstable case ($s(i)>o$) and negative for the stable case, or the unstable waves are sloping toward the west with height and the stable waves towards the east. For the general case which includes heating and friction the sign of θ_T depends on the sign of the numerator in (7.14). This sign must necessarily be positive for the unstable wave due to energy considerations. We consider the available potential energy in the wave. The available potential energy decreases due to the negative generation caused by the Newtonian heating and also due to the conversion from eddy potential to

eddy kinetic energy in the unstable case. Since the eddy available potential energy will increase in this case the conversion from the zonal available potential energy is positive, but this latter conversion is proportional to the heat transport which therefore must be positive. To check this argument the numerator in (7.14) was calculated from the solutions in all unstable cases. The result was invariably positive. In summary, the unstable waves have the temperature field lagging behind the geopotential field, slope towards the west with height and transport sensible heat to the north.

The stable waves are damped in the model and are thus of minor importance. However, for the sake of completeness it should be mentioned that the total heat transport, calculated as the sum of the heat transports of the two solutions given in (7.10), is negative for all (m,n) representing a stable case.

In this section, where we have considered the transient waves as solutions of the linearized equations we have thus arrived at the conclusion that the waves in the unstable case transport sensible heat to the north and slope from east to west with height, while the waves in the stable case transport heat southward and slope eastward with height.

8. CONCLUDING REMARKS

The main result of the investigation is that the structure of long transient and stationary waves are influenced significantly by the strength of the zonal current. Sufficiently strong zonal winds will cause the waves to tilt westward with height, while weak zonal winds will create the opposite slope. This statement applies to the stationary and transient parts of the waves although the mechanisms are different. The slope of the long transient waves are determined mainly by the baroclinic stability of the zonal current while the structure of the stationary part is governed by the influences of heat sources and topography. It has been shown that the latter effects have a generally stabilizing influence on the transient long waves.

While these results are of interest in understanding the observed state of the atmosphere it is interesting to speculate on the implications of the results in medium-range predictions. It is well known that one of the systematic errors in these forecasts is a tendency to merge the polar and sub-tropical jetstreams combined with a general and erroneous strengthening of the zonal winds in middle latitudes. The zonally averaged winds in the high and low latitudes of each hemisphere are decreasing as the forecast progresses in time. Fig.14, kindly provided by Dr. K. Arpe, shows a typical distribution of the errors and the analysed zonal winds in a vertical cross-section from pole to pole for the winter season. The error in the zonal wind may amount to 8-10 ms^{-1} in a 10 day forecast. Given this error and assuming that the simple linear theory developed here is at least qualitatively correct it is to be expected that this systematic error will influence the structure of the very long waves. Although the question deserves a detailed investigation there is already some evidence for the hypothesis.

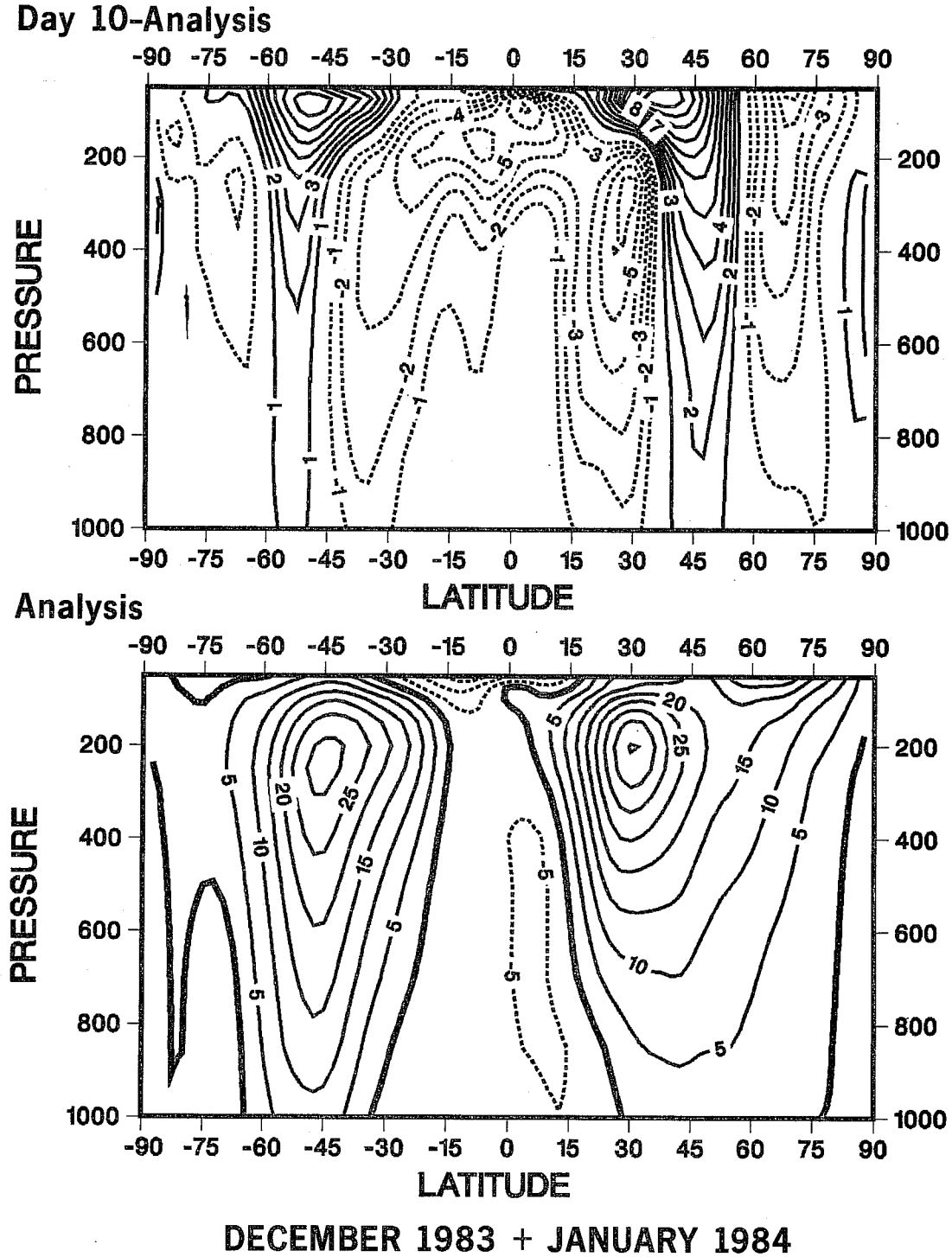

Fig. 14 : The error of the zonally averaged wind in 10-day forecasts as a function of latitude and pressure (top figure). The zonally averaged wind in a similar arrangement (bottom figure). The unit is ms^{-1} in both figures. Period: December 1983 and January 1984.

It was shown in Sect.3 that the maximum relative amplitude in the stationary waves occurs close to the value of n for which the wave is vertical (compare Tables 1b-d with the corresponding part in Tables 2b-d). The position of the maxima in the amplitude were explained as being a resonance phenomenon (see tables after (3.15) and (3.17)), and the resonant wave number becomes smaller as Λ_* and Λ_T increase. One may see this effect in the spectra of the kinetic energy for the observations and for medium-range forecasts prepared by Tibaldi (1984) for the latitude belt 40°-60°N, dominated by too strong zonal winds. The main change during the forecast with the standard orography is a marked increase in the kinetic energy for wavenumber 2 and a decrease for wavenumber 3 interpreted as a shift in resonance. The results of introducing the so-called envelope orography will not be discussed here.

It may also be anticipated that the slope of certain waves may change erroneously during a medium-range forecast. In the high and low latitudes when the zonal wind is decreasing during the forecast it may be expected that a wave changes its slope from a westward to an eastward tilt. An example of such a change can be seen from forecasts prepared by Simmons and Strüfing (1981) (see Fig. 23 in their paper) when the forecasts show a change in the slope of wave number 2 at 60°N from a westward to an eastward tilt.

The major weakness of the present theory is the simplifying assumptions such as the constant angular velocity, the Newtonian form of the heating and the standard parameterization of the dissipation in the planetary boundary layer and the so-called free atmosphere. Needless to say, the use of the two-level, quasi-geostrophic model may also be a restriction.

9. ACKNOWLEDGEMENTS

The author would like to thank Dr. S. Tibaldi who provided the decomposition of the climatological maps in spherical harmonic components, Dr. K. Arpe, who provided additional information from his diagnostic studies. In particular, I want to thank Dr. L. Bengtsson, the Director of ECMWF, for inviting me to the Centre as a visiting scientist.

REFERENCES

Charney, J.G. and A.Eliassen, 1949: A numerical method for predicting the perturbations of the middle latitude westerlies, Tellus, 1, 38-54.

Derome, J.F. and A. Wiin-Nielsen, 1971: The response of a middle-latitude model atmosphere to forcing by topography and stationary heat sources, Mon.Wea.Rev., 99, 564-576.

Eliasen, E., 1958: A study of the long atmospheric waves on the basis of zonal harmonic analysis, Tellus, 10, 206-215.

Haltiner, G.J. and D.E. Caverly, 1965: The effect of friction on the growth and structure of baroclinic waves, Q.J. of the Roy.Met.Soc., 91, 209-219.

Haltiner, G.J., 1967: The effects of sensible heat exchange on the dynamics of baroclinic waves, Tellus, 19, 183-198.

Hollingsworth, A., 1975: Baroclinic instability of simple flow on the sphere, Q.J. of the Roy.Met.Soc., 101, 495-528.

Hollingsworth, A., A.J. Simmons and B.J. Hoskins, 1976: The effect of spherical geometry on momentum transports in simple baroclinic flows, Q.J. of the Roy.Met.Soc., 102, 901-911.

Holopainen, E.O., 1961: On the effect of friction in baroclinic waves, Tellus, 13, 363-367.

Saltzman, B., 1968: Steady state solutions for the axially-symmetric climate variables, Pure and Appl.Geophysics, 69, 237-259.

Simmons, A.. and R. Strüfing, 1981: An energy and angular momentum conserving finite-difference scheme, hybrid coordinates and medium-range weather prediction, Tech.Rep.No.28, ECMWF, 66p.

Smagorinsky, J., 1953: The dynamical influence of large-scale heat sources and sinks on the quasi-stationary mean motions of the atmosphere, Q.J. of the Roy.Met.Soc., 79, 342-366.

Tibaldi, S., 1984: Systematic errors of the ECMWF grid-point forecast models and their relationship with orographic forcing; Riv.Met-Aeron. (in press).

Wiin-Nielsen, A., 1961: On the distribution of temperature relation to height in stationary planetary waves, Tellus, 13, 127-140.

Wiin-Nielsen, A., A. Vernekar and C.H. Yang, 1967: On the development of baroclinic waves influenced by friction and heating, Pure and Applied Geophysics, 68, 131-161.

Wiin-Nielsen, A., 1972: Simulations of the annual variation of the zonally-averaged state of the atmosphere, Geophysica Norvegica, 28, No.6, 1-45.

ECMWF PUBLISHED TECHNICAL REPORTS

No.1 A Case Study of a Ten Day Prediction

No.2 The Effect of Arithmetic Precisions on some Meteorological Integrations

No.3 Mixed-Radix Fast Fourier Transforms without Reordering

No.4 A Model for Medium-Range Weather Forecasting - Adiabatic Formulation

No.5 A Study of some Parameterizations of Sub-Grid Processes in a Baroclinic Wave in a Two-Dimensional Model

No.6 The ECMWF Analysis and Data Assimilation Scheme - Analysis of Mass and Wind Fields

No.7 A Ten Day High Resolution Non-Adiabatic Spectral Integration: A Comparative Study

No.8 On the Asymptotic Behaviour of Simple Stochastic-Dynamic Systems

No.9 On Balance Requirements as Initial Conditions

No.10 ECMWF Model - Parameterization of Sub-Grid Processes

No.11 Normal Mode Initialization for a Multi-Level Gridpoint Model

No.12 Data Assimilation Experiments

No.13 Comparisons of Medium Range Forecasts made with two Parameterization Schemes

No.14 On Initial Conditions for Non-Hydrostatic Models

No.15 Adiabatic Formulation and Organization of ECMWF's Spectral Model

No.16 Model Studies of a Developing Boundary Layer over the Ocean

No.17 The Response of a Global Barotropic Model to Forcing by Large-Scale Orography

No.18 Confidence Limits for Verification and Energetic Studies

No.19 A Low Order Barotropic Model on the Sphere with the Orographic and Newtonian Forcing

No.20 A Review of the Normal Mode Initialization Method

No.21 The Adjoint Equation Technique Applied to Meteorological Problems

No.22 The Use of Empirical Methods for Mesoscale Pressure Forecasts

No.23 Comparison of Medium Range Forecasts made with Models using Spectral or Finite Difference Techniques in the Horizontal

No.24 On the Average Errors of an Ensemble of Forecasts

ECMWF PUBLISHED TECHNICAL REPORTS

No.25 On the Atmospheric Factors Affecting the Levantine Sea

No.26 Tropical Influences on Stationary Wave Motion in Middle and High Latitudes

No.27 The Energy Budgets in North America, North Atlantic and Europe Based on ECMWF Analyses and Forecasts

No.28 An Energy and Angular-Momentum Conserving Vertical Finite-Difference Scheme, Hybrid Coordinates, and Medium-Range Weather Prediction

No.29 Orographic Influences on Mediterranean Lee Cyclogenesis and European Blocking in a Global Numerical Model

No.30 Review and Re-assessment of ECNET - a Private Network with Open Architecture

No.31 An Investigation of the Impact at Middle and High Latitudes of Tropical Forecast Errors

No.32 Short and Medium Range Forecast Differences between a Spectral and Grid Point Model. An Extensive Quasi-Operational Comparison

No.33 Numerical Simulations of a Case of Blocking: the Effects of Orography and Land-Sea Contrast

No.34 The Impact of Cloud Track Wind Data on Global Analyses and Medium Range Forecasts

No.35 Energy Budget Calculations at ECMWF: Part I: Analyses

No.36 Operational Verification of ECMWF Forecast Fields and Results for 1980-1981

No.37 High Resolution Experiments with the ECMWF Model: a Case Study

No.38 The Response of the ECMWF Global Model to the El-Nino Anomaly in Extended Range Prediction Experiments

No.39 On the Parameterization of Vertical Diffusion in Large-Scale Atmospheric Models

No.40 Spectral characteristics of the ECMWF Objective Analysis System

No.41 Systematic Errors in the Baroclinic Waves of the ECMWF Model

No.42 On Long Stationary and Transient Atmospheric Waves